BUSKERUD AND VESTFOLD
HBV
UNIVERSITY COLLEGE

FACULTY OF TECHNOLOGY AND
MARITIME SCIENCES

# Speckle suppression in laser projection displays

Doctoral Thesis

Trinh Thi Kim Tran

2015


**FACULTY OF TECHNOLOGY AND MARITIME SCIENCES**

# Speckle suppression in laser projection displays

Thesis submitted for the degree of Philosophiae Doctor

Trinh Thi Kim Tran

Department of Micro- and Nanosystem Technology (IMST)
Faculty of Technology and Maritime Sciences (TekMar)
Buskerud and Vestfold University College (HBV)
Horten, 2015

Speckle suppression in laser projection displays

Department of Micro- and Nanosystem Technology (IMST)
Faculty of Technology and Maritime Sciences (TekMar)
Buskerud and Vestfold University College (HBV)
Horten, 2015

Doctoral theses at Buskerud and Vestfold University College, no. 4

ISSN: 1894-6380 (print)
ISSN: 1894-7530 (online)
ISBN: 978-82-7860-254-6 (print)
ISBN: 978-82-7860-255-3 (online)



Cover: HBV, Kommunikasjonsseksjonen
Printed at LOS digital

# Preface

This thesis is submitted for the degree of Doctor of Philosophy at the Buskerud and Vesfold University College-Department of Micro and Nano Systems Technology. The financial support is provided by Education Department of Norway (KD), the Research Council of Norway through Lasepro project, the Norwegian Micro and Nano Fabrication Facility (NorFab) and the Norwegian PhD Network on Nanotechnology for Microsystems (NanoNetwork).

# Acknowledgements

I would like to express my special appreciation and thanks to my supervisor Associate Professor Muhammad Nadeem Akram for his valuable advice during my Ph.D. I would like to thank you for encouraging my research and for allowing me to grow as a research scientist. I would also like to thank to my co-supervisors Professor Xuyuan Chen and Professor Einar Halvorsen for their advice and feedback on my research. I also thank to Kjell Einar Olsen and Øyvind Svensen from Projectiondesign AS for their support and useful discussion. I thank to Dr. Guangmin Ouyang and Dr. Zhaomin Tong for their helpful discussion and collaboration.

Special thanks to Nguyen Thai Anh Tuan, Ragnar Dahl Johansen and Zekija Ramic for their help and assistance in the laboratory. Thanks to Tone Gran and Kristin Skjold Granerød for their help on administrative issues. I also thank to my PhD colleagues at HBV for making my time in the PhD program more fun and interesting.

Finally, I take this opportunity to express my gratitude to my parents and my friends for their love, unconditional encouragement and support.

Norway, January 2015
Kim Trinh Tran Thi

# Abstract

Laser light source becomes more popular today in the projection technology. The use of lasers in projection applications provides considerable advantages compared to conventional projection lamps. These are, for example, long lifetime, large color gamut, small étendue for small projection system. However, one of a major obstacles that prevents lasers projection from the market is speckle. Speckle appears as unwanted granular noise on projected images and it degrades the image quality. A number of speckle reduction solutions have been developed in recent years. However, speckle removal methods that can be integrated in laser projection technology are still challenging. The objective of this PhD work is the investigation, application and characterization of methods for speckle suppression in a real laser projection system.

Different approaches for speckle suppression are examined in this work. The first approach is the application of a Microelectromechanical systems (MEMS) diffuser. The benefits of using MEMS diffuser are: less power consumption, small size, simple drive electronics, and simplified integration within a projector. The MEMS diffuser has random patterns that have a role as wavefront phase modulator for speckle suppression. The device is designed based on Silicon on Insulator (SOI) MEMS fabrication process. The design of MEMS diffuser is then theoretical calculated and simulated. The experimental dynamic measurement of MEMS diffuser shows a well fit with the calculation and simulation results. Speckle contrast suppression of the diffuser is characterized. The device provides up to 43.8% of speckle suppression. Based on the same principle, a second generation of MEMS diffuser is designed to have larger height fluctuations with a continuous profile. The calculation, simulation and characterization of the second generation MEMS diffuser are done. However,

due to the properties of fabrication processes, a continuous profile of random patterns can not be attained and therefore the second generation of MEMS diffuser does not offer better speckle suppression.

The second approach for speckle suppression is a commercial phase-randomizing deformable mirror for anti-speckle technology. The mirror can tolerate high optical power thus it is suitable for laser projection system where high power lasers are required. The mirror comprises a continuous surface of micro mirror array that can be individually deformed and actuated up to hundreds of kHz. Due to the deformation of the micro mirrors, speckle contrast is reduced by the introduction of angle diversity. Speckle suppression by combination of wavelength diversity and angle diversity is measured and analyzed. The study is done both for single broadband laser and laser array. It is shown experimentally that speckle contrast can be reduced down to 0.04 for single broadband laser and to 0.033 for four broadband lasers array.

Finally, different speckle suppression methods such as wavelength diversity, angle diversity, moving diffuser are applied in a real laser projection system which is built by Projectiondesign AS. Speckle contrast of the projected images is characterized by setting the camera to match speckle perception of human eyes. Speckle contrast of 0.050 and of 0.038 are attained respectively for red lasers and blue lasers in the projection system.

# Contents

Papers omtitted from file due to publisher's restrictions

# List of publications

## Journal papers

1. T.T.K. Tran, S. Subramaniam, C.P. Le, S. Kaur, S. Kalicinski, M. Ekwinska, E. Halvorsen and M. N. Akram "*Design, Modeling, and Characterization of a Microelectromechanical Diffuser Device for Laser Speckle Reduction*" Journal of Microelectromechanical Systems, volume 23, number 1, page 117–127, July 2013.

2. T.T.K. Tran, X. Chen, Ø. Svensen and M. N. Akram "*Speckle reduction in laser projection using a dynamic deformable mirror*" Optics Express, volume 22, page 11152-11166, 2014.

3. T.T.K. Tran, X. Chen, Ø. Svensen and M. N. Akram "*Speckle reduction in laser projection display through angle diversity and wavelength diversity*"-Draft.

## Conference papers

1. T.T.K. Tran, Z. Tong and M. N. Akram "*Speckle reduction characterization of high power broad-area edge-emitting diodes lasers*" Speckle 2012: V International Conference on Speckle Metrology, Spain, 2012, volume SPIE 8413, page 84131N.

2. T.T.K. Tran, X. Chen, Ø. Svensen and M. N. Akram "*Demonstration of Speckle Reduction in a Laser Projector by Micro-electro-mechanical Diffuser Device*" Frontiers in Optics 2013, Orlando, Florida, 2013, page FM4F.5.

3. M. N. Akram, T.T.K. Tran and X. Chen "*A survey of speckle reduction methods in laser based picture projectors*" International Conference on Optoelectronic Technology and Application 2014 (SPIE).

4. Ø. Svensen, T.T.K. Tran, X. Chen and M. N. Akram, "*Design Aspects for High Lumen DLP Laser/phosphor Projector*" International Optical Design Conference, Kohala Coast, Hawaii United States, 2014, page ITu4C.1

# Chapter 1

# Introduction

## 1.1 Projection Displays Technology

### 1.1.1 Light sources for projection technology

The performance of a projection system is very much dependent on the characteristics of the light sources. There are different available light sources for projection technology such as lamps, light emitting diodes (LEDs) or lasers. Each of them has different characteristics and suitability for different applications.

#### Lamps as projection light sources

The majority of today's projectors use arc lamp which is also known as high intensity discharge (HID) lamp as a light source. A HID lamp consists of a sealed envelope containing the filled materials. HID lamps include Xenon lamp, Metal-halide lamp and ultra high pressure (UHP) lamp [1]. Xenon lamp is a HID lamp that is filled with the noble gas Xenon. Since Xenon is in its gaseous state at room temperature, instant turn on/turn off with no associated warm up period is possible for Xenon lamp. Xenon lamp has a broadband with a relatively flat profile emission in the visible spectrum. Thus, Xenon lamp provides a good colorimetry [2]. Xenon lamp has high brightness therefore it is used in high end large screen cinema projectors

[3, 4].

Another type of HID lamp is Metal-halide lamp. The Metal-halide lamp is filled with mercury and a doping of a halide salt of a desired metal. The characteristics and the spectrum of illumination can be varied by modifying the mixture of metal halide in the lamps [5]. However, the metal halide lamps require long warm-up time to get full brightness and proper color. This occurs because the metal halide salt takes time to be heated up and fully vaporized. Moreover, due to the presence of two or more metals in the lamps, these metals can react with the electrodes and form compounds with lower vapor pressure than the original metal halide [6]. As a consequence, these lamps can change color over the life-time.

The introduction of Ultra High Pressure (UHP) Mercury Hg lamp system by Philips in 1995 is identified as a technological breakthrough for the projection market [7]. Following this launch, the UHP lamps are nowadays most commonly used in the projection technology. The UHP lamps offer a very high luminance with a good spectrum [8]. They are available in version from about $50W$ to $900W$ [6]. One more advantage of the UHP lamps is long lifetime. These lamps can have lifetime of over 10000 hours which is ideal for projection applications [9].

**Light Emitting Diodes (LEDs) as projection light sources**

LEDs are a solid-state emitters that have been currently used as light sources in projectors. Unlike the traditional lamps, LEDs are small and can be switched fast so they do not need warm up time [10]. Moreover, LEDs are now available in all colors for projection applications. The two main advantages of LEDs over UHP lamps are colorimetry and lifetime [11].

Following [6], there are two basic mechanisms for LEDs to produce white light. In the first mechanism, the desired wavelengths can be emitted directly from the LEDs. Consequently, separate red, green and blue LEDs are used to build up a projector. On the other hand, white light can be produced by converting the blue light to the desired wavelength with a Phosphor or Fluorescent materials. Blue LEDs and yellow Phosphor are most commonly used. A part of blue light is absorbed and

excited the yellow light by the yellow Phosphor. The blue light and the excited yellow light mix up to produce white light. Figure 1.1 shows an example spectra of red, green, blue LEDs and white LEDs which is generated by blue LEDs and yellow Phosphor. Unfortunately, the colorimetry of white LEDs which is made by the blue LED and yellow Phosphor is poor. Hence, this LED is only used in the system like cell phone displays where power consumption is paramount and poor colorimetry can be tolerated [6]. Better color can be achieved with a mixture of green and red Phosphors with the blue LEDs. However, these two approaches have lower efficiency than the blue LEDs with yellow Phosphors.

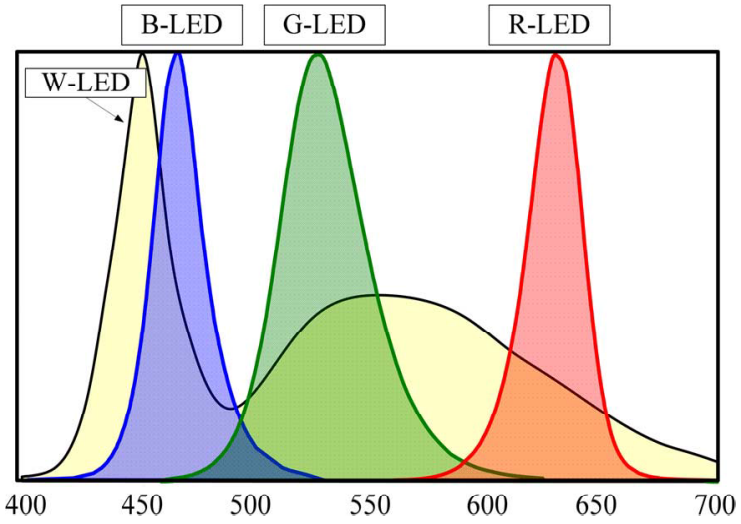


Figure 1.1: Spectrum of red, green, blue LEDs and white LED consists of a blue LED coated with a yellow Phosphor [10]

Due to the lack of filament, LEDs have longer lifetime than traditional lamps for projection displays. In general, the LEDs do not fail catastrophically but their light output decreases slowly over their operating period [12]. Typically, the lifetime of LEDs are about 20.000 hours until the light output drop to 50% of the initial value [13].

Although LEDs provide many advantages, still they have some limits. LEDs have large étendue because of their large emission angle. Hence, it may be challenging for the design of light engine to collect the light from LEDs source without cropping. Besides, the brightness of LEDs is much lower than lamps. This prevents the use of LEDs in the high-output projection systems [14]. However, LEDs have been recently integrated into portable projection systems which high brightness is not required due to the small size [1, 15–17].

**Lasers as projection light sources**

It has been recognized that the conventional lamps have limits both on the performance and lifetime [18]. In addition, LEDs can not be used in the high output projection systems because of low brightness. Thus, lasers are considered as a good light source for new generation of projection systems. After being invented in 1960s, lasers were proposed as light sources for projection use [19]. Since then, laser projectors have not come into production. This is mainly because of high cost of the lasers compared to the lamps. Lasers do not have the same étendue limitation as lamps or LEDs. The very low étendue of the laser would enable very high brightness projection systems to be built with smaller microdisplays [20]. The use of lasers as a light source in projection displays provides a smaller size of projection lens. The maximum effective diameter of the projection lens is reduced by about 40% in lasers-based projection system as compared to the lamps-based projection system [21]. In addition, low divergence angle of the lasers allows the use of low cost-high aperture number $F\#$ number projection lenses [6]. Despite of small size and low étendue, lasers offer very high brightness which is $5 \times 10^6$ times that of LEDs [22]. Lasers also have longer lifetime than lamps and LEDs. It is shown in [23] that the laser's lifetime can exceed 50.000 hours.

A major advantage for laser projection systems is the use of lasers at selected wavelengths that expand the available color gamut to display [24]. With lasers projection displays, the source is monochromatic and within broad limits, lasers of any desired wavelength can be designed. Therefore, it is up to the designer to specify the lasers wavelengths to be used in the projector. The choice of laser wavelengths is based on target color gamut of the display, the availability and cost of the commercial lasers wavelength [6].

Due to these advantages, the light sources for future projection display are believed to be dominated by lasers. But currently, lasers have some problems that must be overcome. The commercial lasers are still far more expensive compared to conventional lamps for being used in mass-market projectors. One more factor needs to be considered is the lasers safety. The lasers are very dangerous for human eyes if they are looked directly. Therefore, it is important that the laser set is sealed in the

projection systems chassis, no direct laser radiation is accessible.

The adoption of lasers in display applications has been limited due to the presence of speckle. Speckle is a consequence of the high temporal and spatial coherence property of lasers and occurs due to the interference of coherent laser light scattered from a random phase delays such as projection screen [25]. Figure 1.2 shows images with and without speckle effect. The original image without speckle is shown in Figure 1.2 (a) which the fine details can be seen clearly. Figure 1.2 (b) shows an image with speckle that appears as a random granular noise superimposed on the intended image, and therefore it significantly degrades the observed images quality. Hence, the suppression of speckle is an important challenge to overcome for the application of lasers in displays technology. More details of speckle properties and methods for speckle suppression are discussed in the next section.

(a) (b)

Figure 1.2: Original image without speckle (a) and image with speckle (b) [26]

### 1.1.2 Digital mirror devices (DMD) for projectors

Digital mirror devices (DMD) is a part of the Digital Light Processing (DLP) system which was produced by Texas Instruments (TI). Since invented in 1987, DMD has come to dominate the projector market [27]. DMD is a MicroEletroMechanical Systems (MEMS) device for fast reflective digital light switch. It consists of a large number of micro-mirrors. Figure 1.3 (a) shows a DMD and an enlarge image of micro-mirrors array is shown in Figure 1.3 (b).

DMD is a spatial light modulator system which uses a number of micro-mirrors to reflect incident light either onto the projection lens or onto a light absorber. The

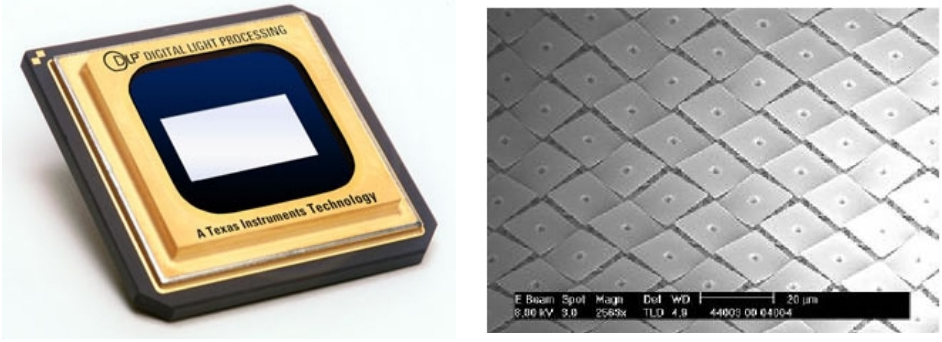


(a) (b)

Figure 1.3: Digital mirror devices (DMD) (a) and a Scanning Electron Microscope image of micro-mirror array (b)

DMD pixel is a micro-mirror that can tilt $\pm 10^o$. The most recent DMD has tilt angle of $\pm 12^o$. The micro-mirrors have two operational states. By convention, the mirror is referred to as the "on" state when the mirror is tilted toward the illumination. When the mirror is tilted away from the illumination, it is referred to as the "off" state. The mirror in the "on" state deflects light from the lamp to the projection lens and the mirror in the "off" state deflects light from the lamp the the light absorber [28]. The required time for the mirror to transit from the "on" position to the "off" position is $20\mu$s [29].

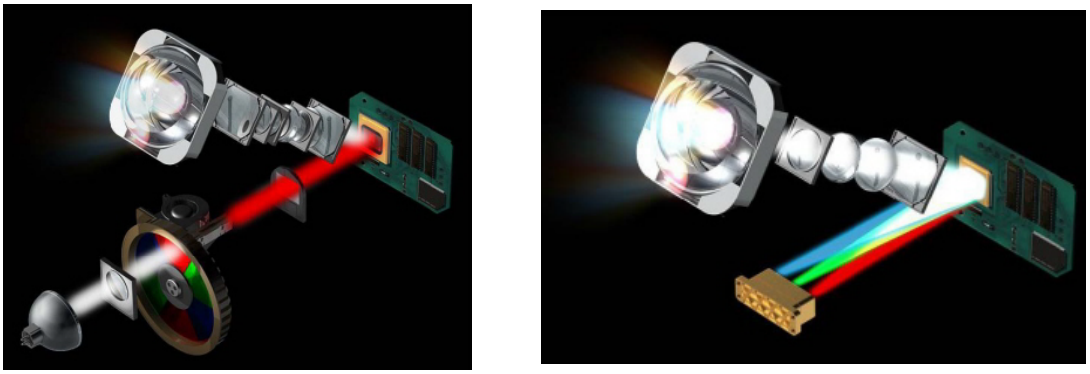

(a) (b)

Figure 1.4: Schematic of lamps projection system (a) and LEDs laser projection system with single DMD chip (b) [22]

Figure 1.4 shows a schematic of lamps and LEDs lasers projection system with single DMD chip [22]. In Figure 1.4 (a), a lamp source requires a spinning color wheel and color filter to add color to the image. The color wheel consists of multiple colors that change the color light coming to the DMD chip. For the LEDs and lasers projection system as shown in Figure 1.4 (b), the primary colors are created directly and therefore a number of optical elements are significant reduced in the system. In

addition, the lack of color wheel and color filter in the LEDs laser projection system provides a better optical efficiency [30].

For both systems, the light from source is directed to illuminate the surface of DMD chip. Depending on the "on" or "off" states of the micro-mirrors, the reflected light from the mirrors is directed either into the pupil of projection lens or away of projection lens respectively. The projection lens collect the light from each "on" state of the mirrors and project an enlarged image to the screen [28].

## 1.2 Speckle and Methods for Speckle Suppression

### 1.2.1 Speckle in lasers projection display

Projection technology plays an important role in modern life. The applications of projection technology can be seen everywhere such as rear-projection televisions, conference room projectors, home theater projectors, cinema projectors, micro projectors etc. With the advancement of the technology, the customers expect higher quality from the projectors such as better resolution, higher brightness, more displayed colors and longer life-time without the need to replace the light source. Lasers are a good candidate as an illumination light source for the projection technology. Lasers offer a number of advantages compared to lamps or LEDs. Lasers provide wider color gamut, better electrical to optical conversion efficiency, higher brightness and contrast of the images and longer life-time [31, 32]

However, an obstacle of lasers in imaging applications is speckle, which is a consequence of the high coherence intrinsic property of the lasers [33, 34]. An illustration of speckle formation is shown in Figure 1.5. A coherent laser beam propagates to a random surface such as projection screen which is considered to be rough on the scale of optical wavelength as illustrated in Figure 1.5 (a). The roughness of the screen surface causes a path difference between individual rays which corresponds to a phase difference of the scattered laser light. As a result, a more or less random electric field distribution is present at the surface. When an observer looks at the laser illuminated screen, the electric field distribution is imaged onto the retina

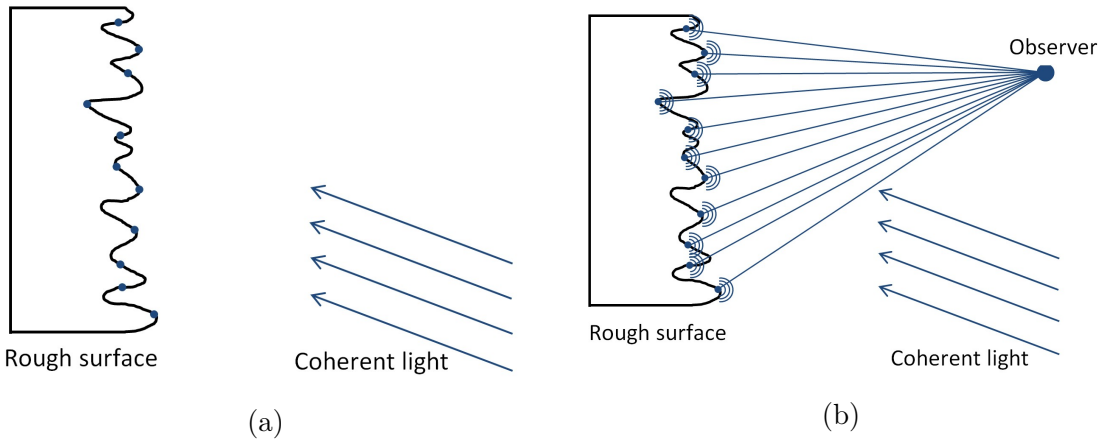


Figure 1.5: Illustration of speckle formation: coherent light propagates to a rough surface (a) and speckle formation from the scattered coherent light (b)

of human eyes, at which interference patterns are formed (Figure 1.5 (b)). As a consequence, the observer will notice random dark and bright granular noise on the intended images. Figure 1.6 shows an image of typical laser speckle patterns.

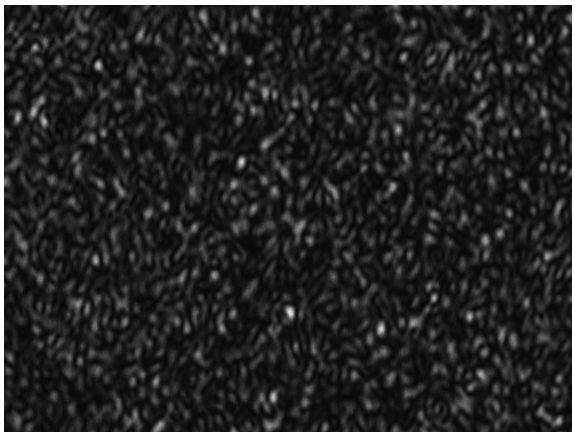

Figure 1.6: Image of laser speckle patterns

The speckle patterns will get smaller or larger if the head of the observer is moved forward or backward respectively. In practice, the speckle size is determined by the spatial resolution of human eyes which is defined as a minimum resolvable distance between distinguishable objects in an image. In addition, the response time of the eyes which is about $1/25s$ should be also taken into account in observations [35]. A slow lateral movement of the eyes corresponds to a very fast movement of the speckle patterns. Human eyes can only recognize speckle with contrast more than 0.04 [36, 37].

Consider a random rough surface is illuminated by a coherent laser beam as shown in Figure 1.5. Each point of the illuminated surface is considered as a secondary source

of scattered electric fields to the observer. The roughness of the random surface causes the optical path difference between the individual scattered rays. Thus, the scattered field has random phases component. In addition, the difference in the distance to the observer, surface reflectivity and the intensity of illuminating light field of each secondary source result random fluctuation amplitude of the scattered field. The resultant field **A** at the observation point is calculated as a sum of random phasor components [38]

$$\mathbf{A} = A\mathrm{e}^{j\theta} = \frac{1}{\sqrt{N}} \sum_{n=1}^{N} a_n e^{j\phi_n} \tag{1.1}$$

where $A$ is the magnitude of the complex resultant, $N$ is the number of random phasor components, $a_n$ and $\phi_n$ are the amplitude and the phase of the $n$th complex phasor components. The intensity of the wavefield $I$ is calculated in terms of the scalar quantity **A** as

$$I = \begin{cases} |\mathbf{A}_x|^2 + |\mathbf{A}_y|^2 & \text{for an unpolarized wave} \\ |\mathbf{A}|^2 & \text{for a polarized wave} \end{cases} \tag{1.2}$$

The variance of the resultant phasor equals to

$$\sigma^2 = \frac{1}{N} \sum_{n=1}^{N} \frac{a_n^2}{2} \tag{1.3}$$

To evaluate the intensity fluctuation resulting from speckles in a speckle pattern, the speckle contrast $C$ is commonly used, and is defined as the ratio of the standard deviation to the mean of the intensity of the pattern, as given by

$$C = \frac{\sqrt{\bar{I}^2 - \bar{I}^2}}{\bar{I}} = \frac{\sigma_I}{\bar{I}} \tag{1.4}$$

where $\bar{I}$ and $\sigma_I$ are the mean value and the standard deviation of the intensity. Under the assumptions that:

1. The amplitude $a_n/\sqrt{N}$ and the phase $\phi_n$ of the $n$th are statistical independent to each other and to the amplitude $a_m/\sqrt{N}$ and the phase $\phi_m$ provided $n \neq m$

2. The phases $\phi_n$ are all uniformly distributed on $(-\pi, \pi)$

Speckle patterns that are generated by a large number of statistical independent phasors $N$ and has speckle contrast $C = 1$ are named fully developed speckle. Fully developed speckle patterns can be generated with a sufficient rough surface, has a Gaussian height distribution and the surface is illuminated with coherent and polarized light. The patterns with suppressed speckle have a smaller value $C$ and the patterns with constant intensity (no speckled fluctuations) have the minimum value of $C$, which is zero.

### 1.2.2 Methods for speckle suppression

For practical application of lasers in projection displays, it is imperative that speckle noise should be reduced below the human perception limit. Human eyes would not be able to recognize the speckle noise on the images if the contrast is less than 0.04 [37]. There are two main mechanisms for speckle suppression. Since speckle is created by the intrinsic coherent property of the laser light, the first mechanism for speckle suppression is to reduce the spatial or temporal coherence of the illuminating laser light. The second mechanism for speckle suppression which is called temporal averaging bases on the limit of the response time of human eyes which is on the order of about $30ms$ [39]. Thus, the change of speckle patterns at high frequency can reduce the visibility of the speckle patterns by temporal averaging of the human eyes. Each mechanism has a variety of methods for speckle suppression. Each method introduces a certain number of degrees of freedom $M$. In general, if $N$ independent methods, each with a degree of freedom $M_n$ are used, the total number degrees of freedom $\mathbf{M}$ is

$$\mathbf{M} = \prod_{n=1}^{N} M_n \tag{1.5}$$

The resulting speckle contrast is

$$C = \frac{1}{\sqrt{\mathbf{M}}} \tag{1.6}$$

#### 1.2.2.1 Speckle suppression by the reduction of spatial and temporal coherence of illuminating lasers

The temporal coherence of a laser is characterized by a so called factor coherence length which is defined as the propagation distance over which a coherence wave maintains a specified degree of coherence. Therefore, coherence length also expresses the optical path length difference of the individual rays. The coherence length $L_c$ is determined in terms of the laser wavelength $\lambda$ and the laser's spectral bandwidth $\delta\lambda$ [40]

$$L_c = \frac{\lambda^2}{\delta\lambda} \tag{1.7}$$

If the coherence length of illuminating laser is less than the surface roughness, the speckle contrast will be significant reduced on the projected images or even speckle free due to the lack of distinct phase relation and the light beams are not able to interfere anymore. Coherence length of white sunlight is approximately $1\mu m$ and of a laser diode is in the range of $500\mu m$ to $1mm$. A highly stabilized gas lasers has coherence length of few hundred meters [41]. The long coherence length leads to the visible speckle with laser light source for projection applications.

**Broadband lasers illumination**

The simplest approach of speckle suppression by the reduction of coherence length is the use of broadband laser. As can be seen in the equation (1.7), the coherence length $L_c$ is inversely proportional to the laser's spectral bandwidth $\delta\lambda$. Broadband laser provides a wide spectral bandwidth and thus shorter coherence length laser beam is attained. This means that the laser beam is less coherent. Thus, speckle contrast is decreased.

A broadband green laser is fabricated based on a Tandem-Poled Lithium Niobiate

(TPLN) crystal [42]. A spectral bandwidth of the laser is shown in Figure 1.7. The laser has bandwidth up to 6.5nm. Due to this broad bandwidth, a low speckle contrast of 0.041 is achieved.

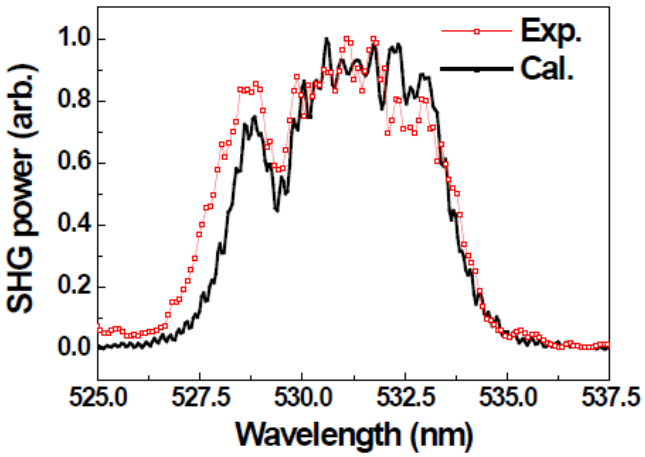


Figure 1.7: Spectrum of TPLN laser at fixed temperature of $39^o$ [42]

White light for projection displays with broad spectrum can also be generated by the blue laser and yellow Phosphor as shown in [43]. A schematic setup of blue lasers and Phosphor is shown in Figure 1.8. Blue lasers are coupled into optical fibers. The output end of the optical fibers is attached to a Phosphor wheel. A part of blue laser beam scatters out through the Phosphor layer and it is converted into yellow light. The combination of blue laser light and the yellow light generates white light that has broad spectrum which provides a low speckle contrast of 0.02.

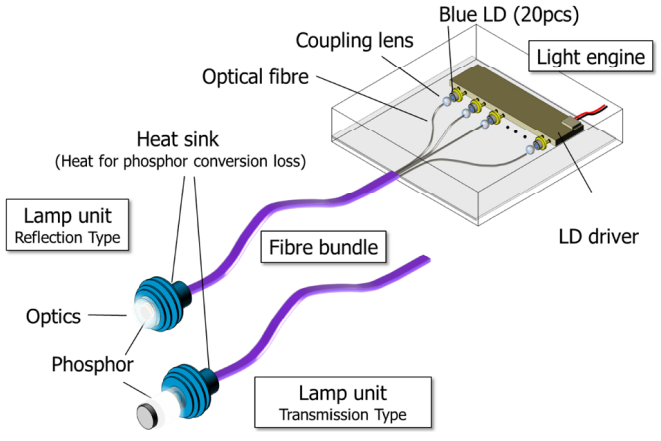


Figure 1.8: Schematic structure of white light generation with blue lasers with Phosphor setup [43]

Laser emission spectrum can also be broadened up to 3.7nm for speckle reduction by tailoring the structure of the laser [44]. An AlGaInP/GaInP quantum well on a GaAs substrate which consists of 25 emitters is modified in the structure. A

schematic structure of standard and modified lasers is shown in Figure 1.9. As can be seen in Figure 1.9 (a), the emitters are evenly spaced on the substrate in the standard laser structure. Under fixed controlled operation temperature, the wavelength distribution of the emitters is uniform with a small deviation which is less than $0.3nm$. The full width at half maximum (FWHM) spectrum width is $0.8nm$ for evenly spaced emitters in the structure and the correspondent speckle contrast is 0.2. Wider spectrum is attained by unevenly spacing of the emitters as illustrated in Figure 1.9 (b). At the small spacing region, the thermal rise is induced and the shift of emitting wavelength is resulted. The spectrum is widened up to $3.7nm$ and speckle contrast is reduced down to 0.05 by this method.

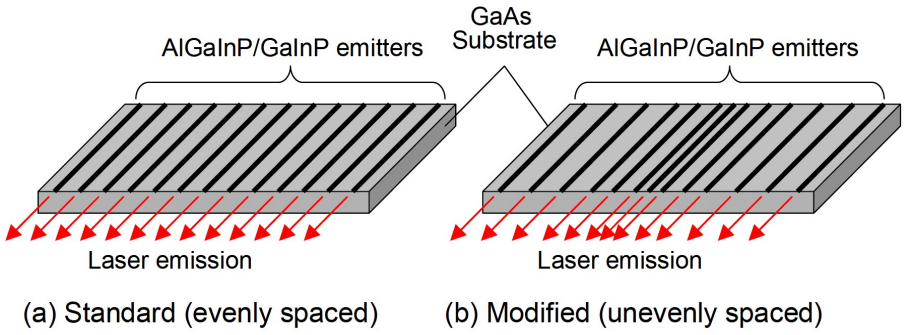


Figure 1.9: Schematic structure of standard-evenly spaced laser (a) and of modified-unevenly spaced laser (b) [44]

### Random laser illumination

Another approach to reduce the coherence length of laser light source for speckle suppression is the use of random laser. As well known, the convention laser trap the light in the cavity which is made of two mirrors. The light is bounced back and forth between the two mirrors and the lasing can only occur at the resonance frequency. Consequently, the emitting laser beam is highly coherent. For a random laser, the light is trapped by a disordered material medium. By multiple scattering of the light in the cavity, a random laser emits its light at many different frequencies and therefore less coherent laser beam is attained by random laser as compared to the conventional laser [45–47]. An efficient speckle suppression is attained by the use of random lasers [48, 49]. Speckle images with a conventional coherent laser beam and with a random laser beam are shown in Figure 1.10. While speckle is clearly visible with conventional coherent laser beam in Figure 1.10 (a), speckle is significantly suppressed with a random laser beam in Figure 1.10 (b).

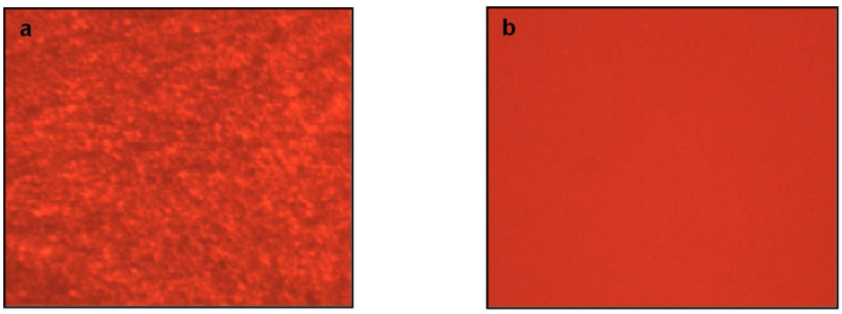


(a) (b)

Figure 1.10: Speckle images of a conventional coherent laser beam (a) and of a random laser beam (b) [48]

### Multiple wavelengths of illuminating lasers

Speckle contrast can also be reduced by using multiple wavelengths of illuminating lasers. Each wavelength produces speckle patterns that become uncorrelated when the difference in wavelength $\Delta\lambda$ satisfies [31]

$$|\Delta\lambda| \geq \frac{1}{2\sqrt{2\pi}} \frac{\bar{\lambda}^2}{\sigma_h} \tag{1.8}$$

where $\bar{\lambda}$ is the mean wavelength and $\sigma_h$ is the standard deviation of the screen surface height. The multiple wavelengths can be provided by one laser source that emits multiple spectral lines as demonstrated in [32]. A frequency-converted green laser is used for speckle suppression demonstration. The laser has spectrum with three spectral lines that have nearly equal intensity and separation of about $0.5nm$. The laser enables speckle contrast reduction with a factor of $\sqrt{3}$. The multiple wavelengths for speckle suppression can also be attained by using different independent lasers light sources as shown in [50–53].

### Optical fiber

Spatial coherence of laser light can be destroyed by temporal coherence with the use of optical fiber. Figure 1.11 shows illustration of optical fiber bundle for speckle suppression which is shown in [54]. The light source is split into many separate beams which are coupled in an optical fiber bundle. The optical bundle consists of a large amount of optical fibers with different lengths. The difference in length of the optical fibers has to exceed the coherence length of the income laser beam. This

results a diverse of optical path delay of the beams. Thus, the laser beam at the output becomes less coherent.

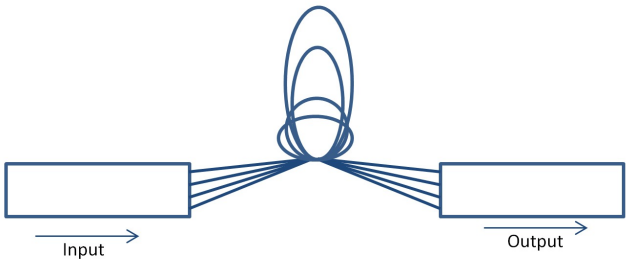


Figure 1.11: Illustration of optical fiber bundle for speckle suppression

The spatial coherence of laser light can be decreased by multimode optical fiber. Theoretical approach of speckle suppression by multimode optical fiber is presented in [40,55]. The multimode fiber arises from the differences among the group velocities of the modes. This results in a spread of travel times and results in the broadening of a light pulse as it travels through the fiber. Consequently, the light becomes less coherent at the output of the fiber. Speckle patterns in the multimode fiber is affected by the length of the fiber $L$. With Gaussian spectrum light source, speckle contrast at the output of multimode fiber is calculated as [40]

$$C = \frac{1}{L^2}\left[1 + \frac{\pi^2}{6}\frac{L^2\left(NA\right)^4}{n_1^2}\frac{\Delta\lambda^2}{\lambda^2}\right]^{-\frac{1}{2}} \tag{1.9}$$

where $NA$ is the numerical aperture of the fiber, $n_1$ is the reflective index of the fiber's core, $\lambda$ is the central wavelength of the laser and $\Delta\lambda$ is calculated in terms of $1/e$ half-width of the laser spectrum $\Delta\nu$ and speed of light $c$ as

$$\Delta\lambda = \frac{\Delta\nu\lambda^2}{c} \tag{1.10}$$

**Ferroelectric Cell**

One method for speckle suppression by using an electrooptical cell which is fill with smectic Ferroelectric Liquid Crystal (FLC) is demonstrated in [35]. The central mass of FLC molecules is periodically ordered along long axes of the molecules. The molecules have their initial polarization. When a voltage is applied, the polarization

is changed according to the direction of the electric field. Consequently, a spatial deformation of the FLC and corresponding to random variations in the refractive index in the FLC is generated by applying pulse wave voltage to the cell. This results a random change in spatial phase of the passing light. Hence, the laser beam is less coherent and speckle is reduced. It is demonstrated that 50% of speckle reduction can be achieved by this method.

#### 1.2.2.2 Speckle suppression by temporal averaging

This is one of the most common approach for speckle suppression by generating time-varying speckle patterns to superimpose upon the amplitude image [56]. The time-varying speckle patterns are generated due to the movement of optical structure such as moving diffuser, moving lens array or moving screen. If the speed of change is beyond the recognition level of human eyes, speckle contrast would be averaged out.

**Vibrating diffuser**

The vibrating diffusers are frequently used for speckle reduction in projection display technology. By the vibration of the diffusers, the degree of temporal coherence is destroyed and this leads to the reduction of speckle contrast. Coherence theory approach of a laser beam passing through a moving diffuser is presented in [57]. Vibrating diffuser for speckle suppression in pico-projector application is presented in [58]. Figure 1.12 shows the setup layout. There are two diffusers which are placed just before and after the light pipe. In order to avoid the blur projected images, only the first diffuser before the light pipe is vibrated horizontally by a Voice Coil Motor (VCM) oscillator. With frequency $100Hz$, the vibrating amplitude is $0.5mm$. The vibrating diffusers can be found with different divergent angles $(5^o, 10^o, 30^o)$. It is proven that better speckle contrast is attained with larger divergent angles of the diffusers. Speckle contrast of 0.0281 with divergent angles of $30^o$ for both diffusers is demonstrated by this method.

The diffuser can have pure sinusoidal vibration as shown in [59]. The glass diffuser which is shown in Figure 1.13 is activated by a tuning fork. It is explained theo-

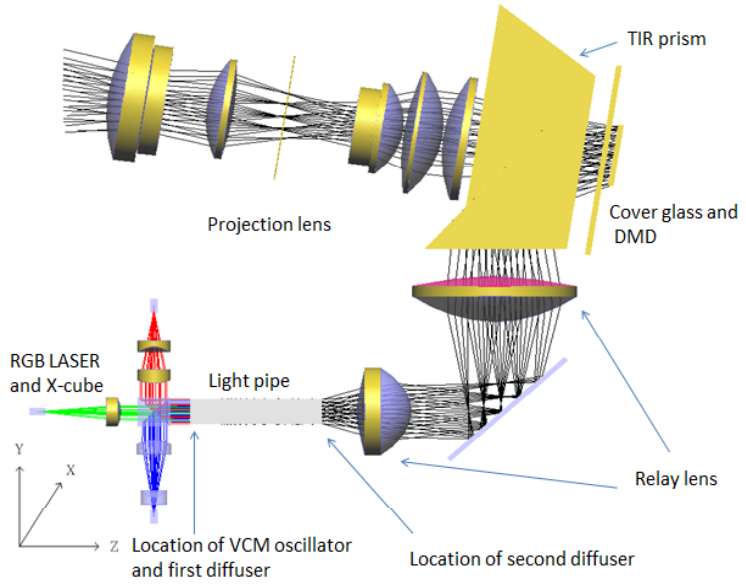


Figure 1.12: Layout of speckle suppression by vibrating diffuser in pico-projector [58]

retically if the vibration of the diffuser is pure sinusoidal, the temporal degrees of freedom becomes extremely large. Therefore speckle contrast depends mainly on the spatial degree of freedom $K$ which is determined by the ratio of the projection lens numerical aperture and the observer eyes numerical aperture. The value of $K$ can be in a range of 500-10000 for typical projection lens [40]. By using this method, speckle contrast is brought down to 0.034 experimentally.

Figure 1.13: Glass random diffuser

### Colloidal dispersion

Speckle suppression by using a colloidal dispersion is presented in [47]. The motion of colloidal particles at room temperature acts as a moving diffuser. Due to the motion of the colloidal particles, uncorrelated speckle patterns are generated and

thus speckle contrast is reduced. A colloidal solution that consists of $TiO_2$ was used for the measurement in the paper. The $TiO_2$ particles have radius of $205nm$. A sketch of laser beam from a single mode optical fiber (SMF) illuminates the colloidal solution is shown in Figure 1.14. The fiber tip is at a distance $L$ from the bottom of the cuvette and the thickness of colloidal solution in the cuvette is $t$. From the experimental measurement, the paper shows that lower speckle contrast is attained with the increase of $L$. Unfortunately, the increase of $L$ leads to the decrease of the transmission light intensity. Speckle contrast of 0.032 is achieved with $L = 5mm$ in the paper.

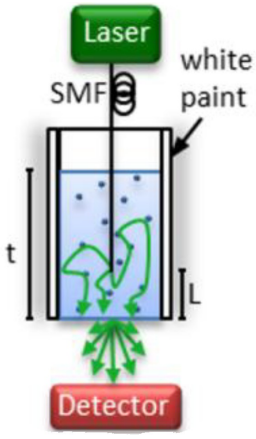


Figure 1.14: Schematic of colloidal solution which is illuminated by a laser with single mode optical fiber [47]

### Rotating diffuser

The temporal average of speckle patterns can also be achieved by the rotation of diffusers. Speckle suppression by rotating diffuser in Liquid-crystal-on-silicon (LCOS) laser projection system is investigated in [60]. The divergent angle of the diffuser is between $0.5^o$ to $1^o$. This method shows a speckle suppression from 0.2 to 0.05 in the LCOS system.

### Rotating lens array

A rotating lens is used for speckle reduction in [61] by creating angle diversity. Figure 1.15 shows a schematic illumination optics with rotating lens array. The rotating lens array is placed in front of the rod integrator. Thus, various incident angles of laser beams propagate to the rod integrator after passing through the lens array. Significant speckle suppression is realized by this method.

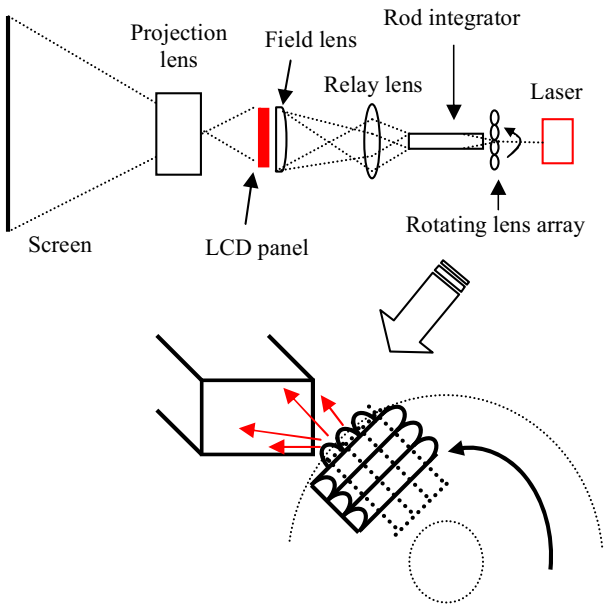


Figure 1.15: Schematic illumination optics with rotating lens array [61]

### Light modulator

Another approach to generate time-varying speckle patterns is the use of light modulator. Light modulator can be diffractive optical elements (DOE) which is investigated for speckle suppression in [62, 63]. Figure 1.16 shows an illustration of DOE. The coming light is split into different diffractive orders which is denoted as 0, $\pm 1$ in the Figure 1.16. The thickness of cells modulator has to satisfy $h\,(n_0 - 1) = \lambda/2$ where $\lambda$ is the wavelength of laser and $n_0$ is the reflective index of the modulator's materials. Speckle contrast is reduced by the vibration of the DOE which creates different phase shifts for different diffrative orders.

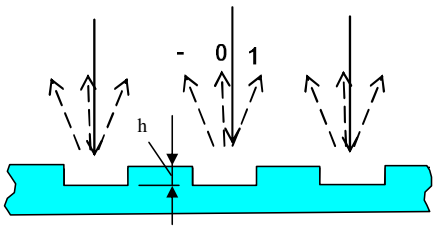


Figure 1.16: Illustration of diffractive optical element [62]

An application of dynamic diffractive optical element (DDOE) for speckle reduction is presented in [64, 65]. Figure 1.17 shows a schematic drawing of DDOE which consists of one or several spatial light modulator (SLM) gratings. When the SLM gratings are activated, an income laser beam is split into several diffractive beams by

the deform of the polymer layer. These diffractive beams create time varying speckle patterns through angle and spatial diversity and this helps to reduce speckle. The speckle patterns are independent if there is no overlapping areas between the diffractive beams on the diffuser. The SLM gratings can have different angles of diffraction due to the difference in angle of the electrodes on the SLM gratings. Number of independent speckle patterns are introduced by the DDOE can be calculated in terms of the number of SLM gratings $m$

$$M = 2^m \tag{1.11}$$

However, the number of SLM gratings can be used in the system is limited since the overlapping of diffractive beams may happen with the increase of number of SLM grating.

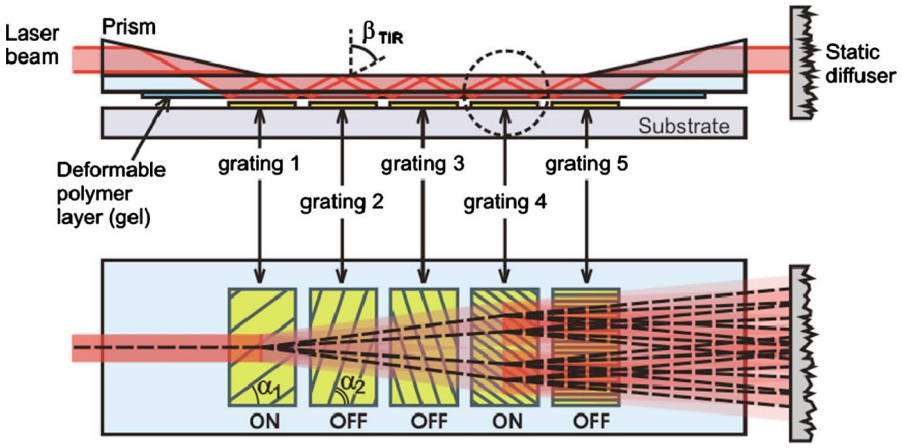


Figure 1.17: Drawing of dynamic diffractive optical element [65]

### 1.2.3 Research Focus

The solution for speckle suppression is very important for the applications of laser projection displays. Despite of much effort and significant progress in recent years, approaches for speckle suppression that can be used in real projection system is still a challenge. This PhD work is focused on the development of practical methods and solution for speckle suppression for the Digital Micromirror Device (DMD) laser projector. There are two main tasks in the project. The first task is the investigation of speckle suppression methods and the second task is the application and characterization of speckle suppression methods in a laser projection system.

**Study 1: Investigation of speckle suppression methods**

Different approaches for speckle suppression by destroying the spatial and temporal coherence of lasers are investigated:

1. Vibrating diffuser-Journal paper 1 and Conference paper 2

A vibrating MEMS diffuser with random phase modulator for speckle suppression is designed, calculated, simulated and characterized. Due to the sinusoidal vibration of the diffuser at high frequency, time-varying speckle patterns are generated. These time-varying speckle patterns are averaged by the limit of spatial and temporal response time of human eyes which is about $30ms$.

2. Deformable mirror-Journal paper 2 and draft of Journal paper 3

A commercial phase-randomizing deformable mirror for anti-speckle technology is studied for speckle suppression. The mirror comprises of continuous surface of mirrors array that can be individually deformed and actuated up to hundreds of kHz. The mirror provides high reflection efficiency over the range of visible wavelengths and can tolerate high optical power. Due to the randomly distributed deformation at high frequency, many uncorrelated speckle patterns are produced and this leads to the reduction of speckle contrast in the projected image.

3. Speckle suppression by wavelength diversity-Conference paper 1

The dependence of speckle contrast on the driving condition is studied. The lasers are driven with continuous wave as well as pulse wave with different duty cycles and driving currents. In addition, wavelength diversity for speckle suppression by the use of different independent laser sources is also characterized and analyzed.

**Study 2: Application and characterization of speckle suppression methods in laser projection system**-Conference paper 4

A laser/Phosphor projection system is built by Projectiondesign AS. The system uses high power red and blue lasers. The Phosphor is used to generate the green light due to the high price of the green lasers. By using of blue lasers as excitation source, yellow light is attained when the blue light passes through the Phosphor. Thus, green light is produced by the combination of yellow light and blue light.

As using laser sources, the projection system has speckle problem. Different methods for speckle suppression are applied in the system such as angle diversity, wavelength diversity, moving diffusers. The speckle contrast of the speckle suppression methods in the projection system is examined.

# Chapter 2

# Summary of Research Work

## 2.1 Microelectromechanical (MEMS) diffuser for speckle suppression-First generation

### Journal paper 1

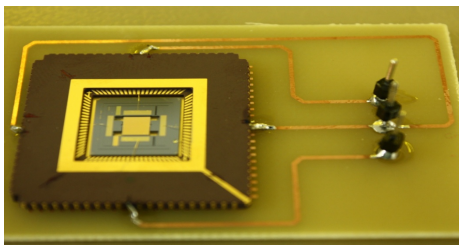

Figure 2.1: Packaged chip mounted on PCB for external connections

Speckle suppression by temporal averaging is the most used approach for speckle suppression. This method reduces speckle contrast by producing time varying speckle patterns within the integration time of human eyes. Despite of much effort and significant progress in recent years for speckle suppression by temporal averaging, current implementations of this method in a real projector are in themselves quite bulky requiring a comparative large optical system. As a solution to the miniaturization challenge, a MEMS moving diffuser with random reflective pattern for speckle suppression is investigated. Figure 2.1 shows a MEMS diffuser device. The device is attached to a chip carrier which is mounted on a printed circuit board (PCB) for external power connection. The MEMS technology is used due to its

benefits such as less power consumption, smaller size, simple drive electronics, and simplified integration within a projector.

### 2.1.1 Device Design and Description

#### Device Description

The fabrication of the device was done by MEMSCAP in their multi-project-wafer service using Silicon on insulator Multi-User MEMS Process (SOI-MUMPs). The device consists a device layer on top of a buried oxide layer and handle layer. The device layer in which the moving mass, comb fingers and the springs are formed have a thickness of $25\mu m$. The buried oxide layer between the silicon device layer and handle-wafer substrate provides a good electrical insulation between the structures and the substrate.

Figure 2.2 (a) shows top-view of the MEMS diffuser device with the moving mass suspended by four folded flexure springs and the two comb-drive transducer structures. The close-up of the spring and the comb-drive structure pictures are shown in Figure 2.2 (b) and Figure 2.2 (c) respectively. The comb-drive structure has a design of $6\mu m$ of fingers width and the designed gap between the fingers is $5\mu m$. The surface of the moving mass has metal reflecting layer with random height distribution (Figure 2.2 (d)). All the dimensions of the diffuser device are shown in Table 2.1.

Table 2.1: Designed structure dimensions

| Description | Dimension |
|---|---|
| Device layer thickness $h$ | $25\mu m$ |
| Proof mass dimensions | $3.5mm \times 3.5mm$ |
| Width of the fingers | $6\mu m$ |
| Gap between the fingers $d$ | $5\mu m$ |
| Length of the fingers | $160\mu m$ |
| Initial finger overlap | $80\mu m$ |
| Number of fingers at each side of the mass $n$ | 159 |

The top surface of the moving mass has a reflective metal layer which consists of a Chromium (Cr) adhesive layer and a Gold (Au) layer with random height distribution. The random patterns have a role as wavefront modulator for speckle

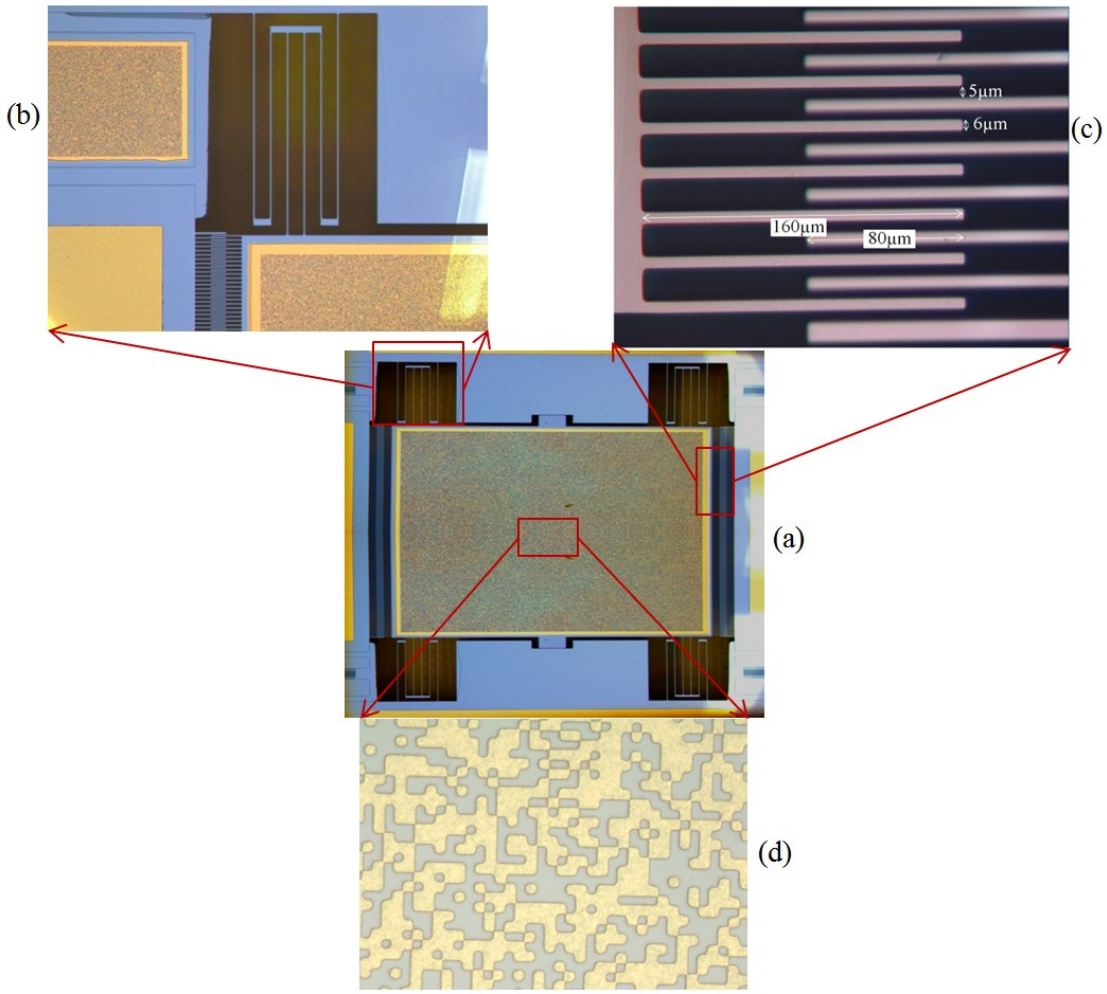


Figure 2.2: Top-view of the MEMS diffuser device (a), zoom in of the spring (b), comb-drive structure (c) and the random patterns on top of the mass (d)

reduction given in. The random reflective patterns of the diffuser consists of pseudo-random pixelated square patterns of height variation that are micromachined on the surface of the diffuser. The random patterns have pixel size of $4\mu m \times 4\mu m$. This size was chosen under consideration of design rules of MEMSCAP. Figure 2.3 (a) shows a top-view picture of the random patterns which was captured by white light interferometer. The height difference of the random patterns was measured to be $500nm$ as shown in Figure 2.3 (b).

### Spring Design

For this MEMS diffuser device, the two most important dynamic properties are the resonance frequency and displacement amplitude of the moving mass. These two components mainly depend on the thickness of the structure, the gap between the transducer fingers and the stiffness of the spring. Since the thickness of the structure

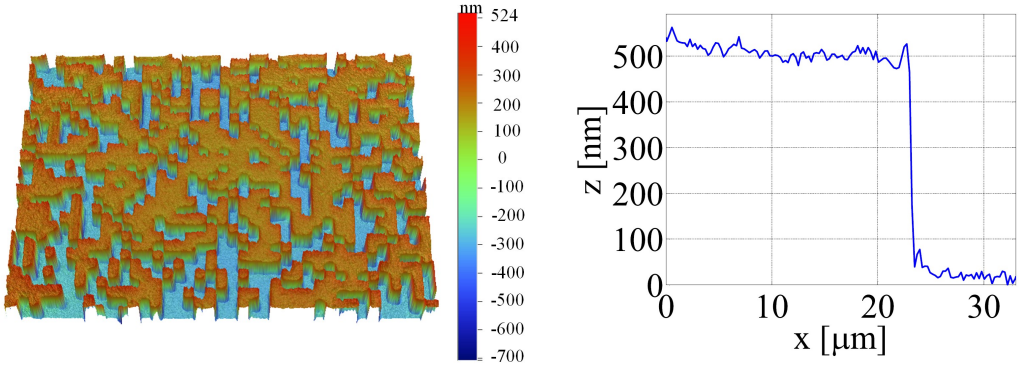


(a) (b)

Figure 2.3: Top-view of random pattern on top of the moving mass (a) and height measurement of random pattern step (b)

and the minimum gap of transducer fingers are fixed by the fabrication process, the design of the spring is therefore the main focus of the design procedure. The quad folded flexure structure is used for the spring design to have linear response to avoid any harmonics in the motion of the diffuser. A sketch of the structure is shown in Figure 2.4 (a). The aim of spring design is to make it more compliant along the $x$-direction for in-plane movement and highly stiff along the $z$-direction to avoid the out of plane movement. The stiffness of the spring in the $x$-direction and the $z$-direction are given by

$$k_x = 2Ehw^3 \left( \frac{1}{L_{EF}^3 + L_{AB}^3 + L_{CD}^3} \right) \tag{2.1}$$

$$k_z = 2Ewh^3 \left( \frac{1}{L_{EF}^3 + L_{AB}^3 + L_{CD}^3} \right) \tag{2.2}$$

Where $E$ is the Young's modulus, $w$ is the width of spring beam, $h$ is the thickness of the structure, $L_{EF}$, $L_{AB}$, $L_{CD}$ are the length of the spring beams as shown in Figure 2.4 (b).

For projection systems with DMD chip, the frame rate range is 30-60Hz. The frame rate defines the number of images which are displayed in a second by the projection system. That means the time for one frame is from $33.3msec$ to $16.6msec$. The motion of the diffuser is cyclic, thus the same speckle pattern is generated after one cycle. Consequently, the resonance frequency of the diffuser should be higher than

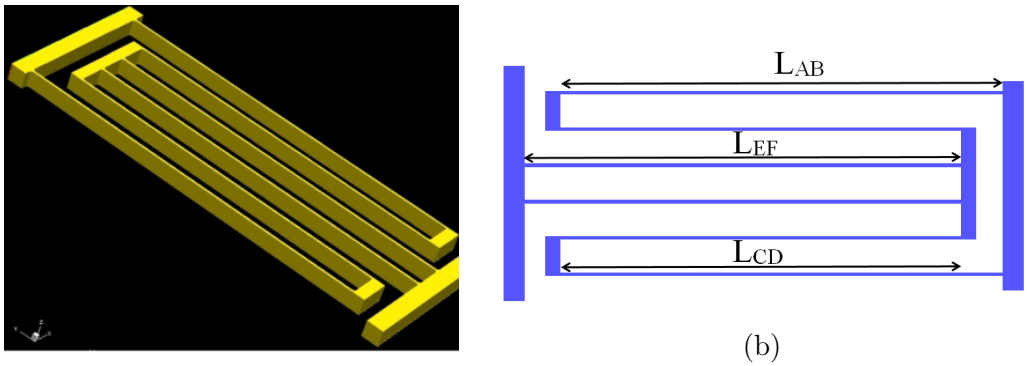


(a) (b)

Figure 2.4: Quad folded flexure spring beam structure (a) and spring dimension (b)

the frame rate value in order to have necessary speckle reduction within one frame time. Besides, if the resonance frequency is too low, the springs are too soft and may cause bending under the weight of the mass. Hence, the resonance frequency of the diffuser is designed to be 300Hz. It means that one moving cycle would be completed in $3.33msec$ which is smaller than the frame time. The designed dimension of the spring is shown in Table 2.2. The calculated stiffness of one spring in the $x$-direction and in the $z$-direction are $k_x = 0.888N/m$ and $k_z = 11.33N/m$ respectively.

Table 2.2: Designed dimensions of the spring

| Spring length | Dimension |
|---|---|
| $L_{EF}$ | $1050\mu m$ |
| $L_{AB}$ | $1065\mu m$ |
| $L_{CD}$ | $965\mu m$ |

**Residual stress characterization**

By using white light interferometer, the deformation of the springs and the curvature of moving mass are estimated. The departure from a flat surface of the mass and the springs causes change in the behavior of the MEMS device, for example the measured resonant frequency and vibration amplitude would be different from the simulated values. The curved surface is due to the residual stress in different layers in the fabrication process. In order to determine the deformation caused by the stress, the stress simulation using Coventor's MEMSMech module is done. Figure 2.5 (a) shows the simulated deformation of moving mass under the residual stress. From the simulation, it can be seen that the stress causes displacement at the center of the mass. White light interferometer measurement is done in a real device to determine the curvature and the displacement in the $z$-direction of the moving mass.

The displacement in the $z$-direction along the $y$-direction of the mass is shown in Figure 2.5 (b). The result shows $10.5\mu m$ of $z$-displacement of the mass and the $8.9\mu m$ more at the center compare to the edge of the mass.

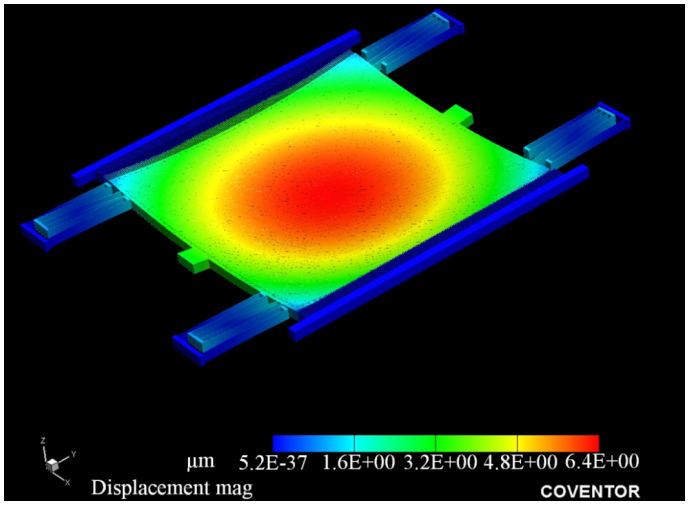


(a)

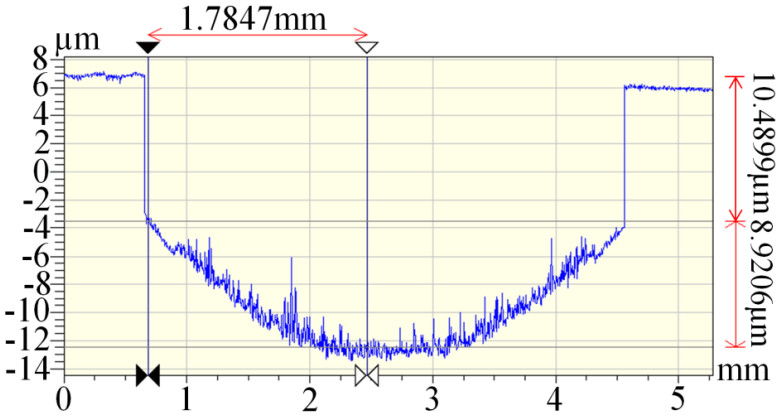


(b)

Figure 2.5: Curvature of moving mass due to the residual stress determined by CoventorWare simulation (a) and white light interferometer measurement (b)

### 2.1.2 Dynamic Characterization

#### Resonance Frequency Characterization

In order to have a large displacement of the moving mass, the MEMS diffuser is driven at the resonance frequency. A stroboscopic interferometer method is used to determine the dynamic properties such as the resonance frequency, vibration mode shape and amplitude. By measuring the displacement of the moving mass with a frequency sweep, the resonance frequencies are determined. Figure 2.6 shows the

measurement of resonance frequency of two device samples. The measured resonance frequencies are 298.1Hz and 298.6Hz which are quite close to the designed value 300Hz.

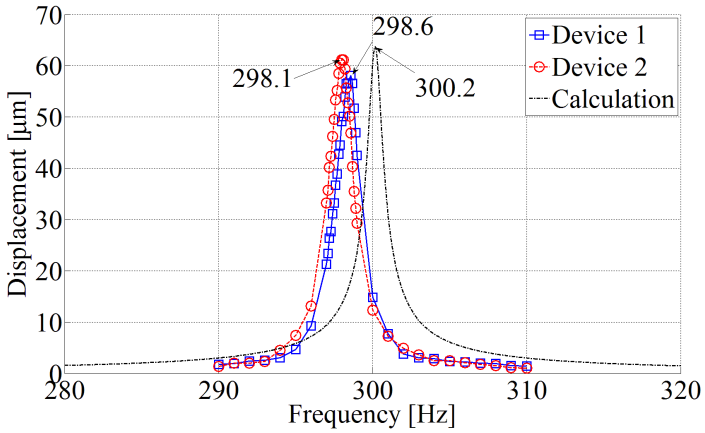


Figure 2.6: Resonance frequency determination

### Displacement Waveform Characterization

For speckle suppression, it is important that the displacement of the moving mass has a pure sinusoidal in-plane motion so that the introduced temporal degree of freedom becomes extremely large [59]. Therefore, the displacement waveform of the moving diffuser is estimated by measuring the displacement in time of the moving mass at resonance frequency. A plot of measured displacement with fitting curve is shown in Figure 2.7.

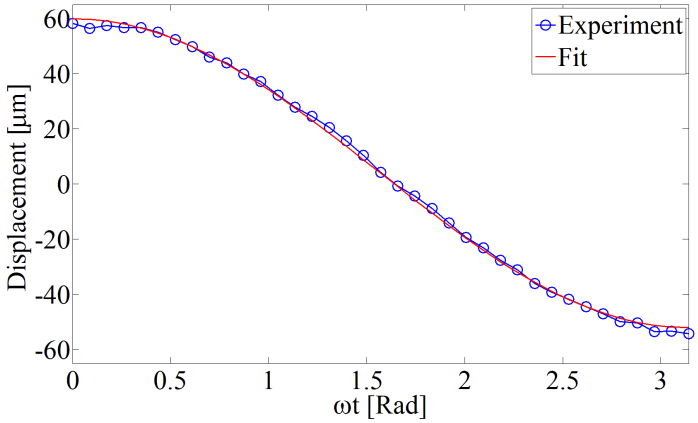


Figure 2.7: Displacement of moving mass at resonance frequency

The measured displacement is fit to the equation

$$x(t) = x_o sin(\omega t - \varphi) + x_1 \tag{2.3}$$

with parameters $x_o = 55.97\mu m$, $x_1 = 3.913\mu m$ and $\varphi = \pi/2$ . The displacement is well approximated by the sinusoidal waveform. The offset of $3.913\mu m$ is caused by the resolution of the camera.

### 2.1.3 Speckle contrast suppression characterization

Speckle contrast suppression is characterized for two different setup: freespace geometry setup and light pipe geometry setup. A narrow bandwidth He-Ne red laser with $4mW$ power and wavelength of $633nm$ is used for the measurement. After passing through two polarizers for the control of polarization and the intensity of the transmitted beam, the laser beam is reflected by the vibrating random surface of the MEMS diffuser device with an angle of $45^o$.

For freespace geometry setup, the reflected laser beam from the MEMS diffuser is imaged on a transparent random surface by an objective lens with a focus length $f = 50mm$ with unit magnification. The random diffuser is made from glass and has a $120\mu m$-grit sandblasted surface. Finally, the beam reached the Charge Coupled Device (CCD) camera where the speckle image is captured without any imaging lens. The resolution of the CCD camera is $640 \times 480$ pixels and each pixel has a dimension of $5.6\mu m \times 5.6\mu m$.

For light pipe geometry setup, the reflected laser beam from the MEMS diffuser is scattered by a stationary random plate to initially homogenize the beam. The scattered beam is then passed through a rectangular light pipe for further beam homogenization by the multiple reflection of the light beam at the walls of the light pipe. The light pipe has a cross section of $7mm \times 5mm$ and a length of $40mm$. Further laser beam homogenization is done by placing another stationary random surface plate at the other end of the light pipe. The speckle image is captured by a CCD camera which is equipped an imaging lens. The imaging lens has focal length of $f = 75mm$. In order to increase the magnification of the captured images, a extended tube with a length of $75mm$ is used.

A MEMS device is driven at the resonance frequency for speckle suppression characterization. The displacement of the moving mass is controlled by changing the

driving voltage. The result of speckle contrast measurement for freespace geometry setup is shown in Figure 2.8 (a). Taking the speckle contrast value when the diffuser is stationary as the reference value, the maximum speckle contrast suppression at maximum displacement ($5V$ AC bias-$25V$ DC bias) is 43.8%.

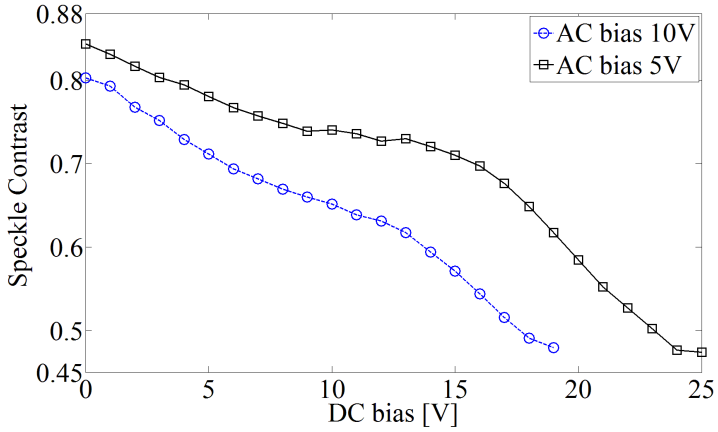


(a)

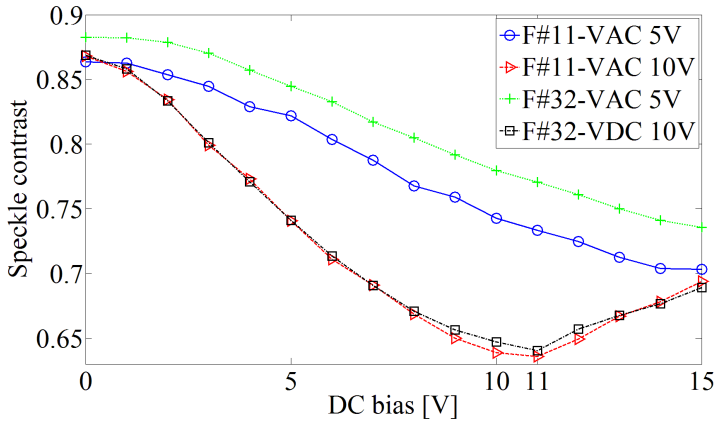


(b)

Figure 2.8: Speckle contrast measurement of freespace geometry setup (a) and light pipe geometry setup with aperture number $F\#11$ and aperture number $F\#32$ (b)

For the light pipe geometry, speckle suppression characterization is performed with two different aperture-number $F\#11$ and $F\#32$ of the imaging lens controlled by an iris inside the camera lens. Since speckle size depends upon the $F\#$ of the imaging camera, thus by varying the aperture-number $F\#$, the speckle size is changed. With higher $F\#$ number, the iris of the imaging lens becomes smaller and the speckle size becomes larger. Up to 26.8% and 26.3% of speckle contrast suppression are achieved with $10V$ AC bias and $11V$ DC bias for $F\#11$ and $F\#32$ respectively. A plot of measured speckle contrast with the change of bias voltage for light pipe geometry is shown in Figure 2.8 (b). At a fixed $AC$ bias voltage and $F\#$, speckle contrast value is largest with the stationary diffuser. By increasing DC bias, the displacement

amplitude increases leading to a reduction of speckle contrast. However, speckle contrast shows an inflection point at $10V$ $AC$ bias. It reaches a minimum value at $11V$ $DC$ bias, then starts increasing as the DC bias is increased further. At small bias, the movement of diffuser has sinusoidal wavefront which is the critical condition for maximum speckle contrast reduction. Thus, speckle contrast reduces with the increase of displacement amplitude and reaches to the minimum values at $DC11V$ and $AC10V$ bias. If the applied DC bias is too large, the random surface diffuser starts hitting the end-stop. Hence, the displacement is no longer sinusoidal and the speckle contrast therefore increases. Images of speckle pattern for free space geometry setup without speckle suppression and with speckle suppression by moving diffuser are shown in Figure 2.9.

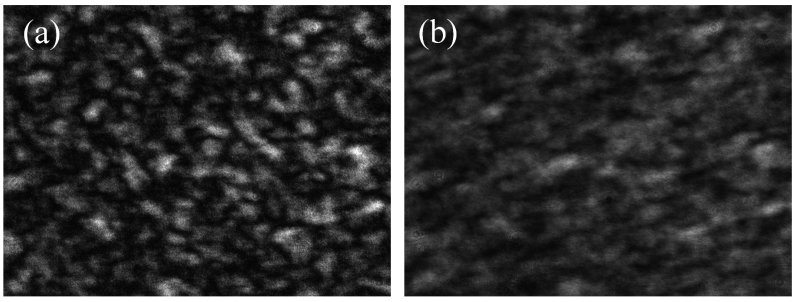


Figure 2.9: Speckle images for freespace geometry of stationary diffuser (a) and of moving diffuser (b)

### 2.1.4 Demonstration of speckle suppression by MEMS diffuser in a laser projector

#### Conference paper 2

In order to demonstrate speckle suppression by the MEMS diffuser, speckle contrast suppression in a commercial projector is investigated. Figure 2.10 shows the setup of the demonstration. A blue Nichia NDB7675 with optical power of $1.4W$ at $1.2A$ of driving current is used for the demonstration. The laser is driven at fixed temperature of $25^oC$. The demonstration is built on a $F2SX+$ wide projector from Projectiondesign AS. The laser beam is illuminated on the surface of MEMS diffuser. After passing through the optical systems of the projector, the picture is imaged on a screen. For speckle contrast calculation, the speckle images are captured by a CCD camera which has $1600 \times 1200$ pixels and the pixel size is $4.4\mu m \times 4.4\mu m$.

The camera is equipped with an imaging lens that has focal length of $50mm$ and the aperture number $F\#$ is 16. The MEMS diffuser is driven at the resonance frequency by applying sinusoidal $AC$ and $DC$ voltage to the comb-drive transducer structure.

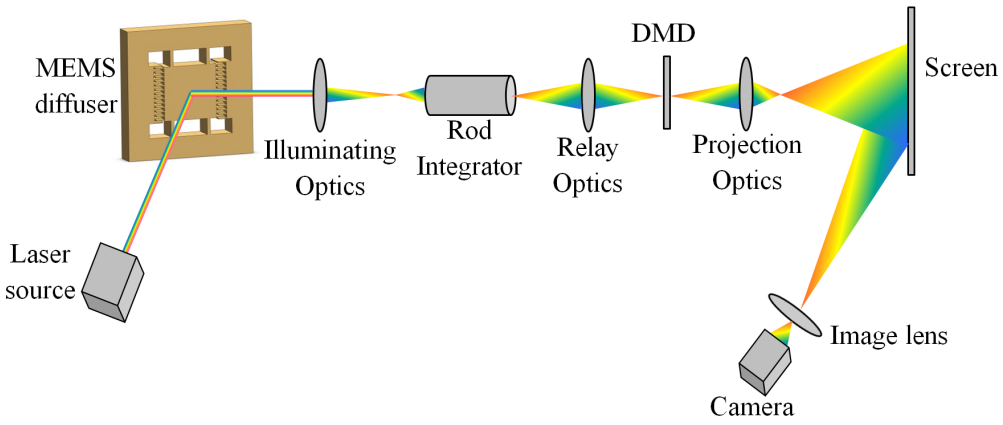


Figure 2.10: Experiment setup for demonstration

By fixing the $DC$ voltage at $5V$, the $AC$ voltage is varied from $0V$ to $10V$. This corresponds to a displacement of $\pm 56.5\mu m$ of the moving diffuser. The result of speckle contrast measurement is shown in Figure 2.11. With stationary diffuser (at $0V$ $AC$ bias), the value of speckle contrast is 0.4708 which is smaller than the theoretical value 0.707. This is resulted by less coherent laser beam due to the wide spectrum bandwidth. Speckle contrast reduces to 0.3070 at $10V$ $AC$ bias. This is equal to 34.8% of speckle reduction.

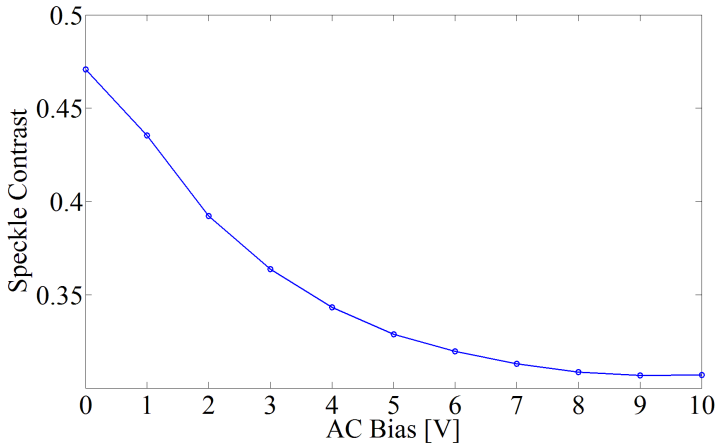


Figure 2.11: Speckle contrast with the change of AC bias

Images of the projected picture on the screen without speckle suppression and with speckle suppression are shown in Figure 2.12 (a) and Figure 2.12 (b) respectively. In order to have an image of full screen, a Nikon camera with $50mm$ focal length of

image lens is used for the capture. The exposure time is $1/3s$ and aperture number $F\#$ is 1.8.

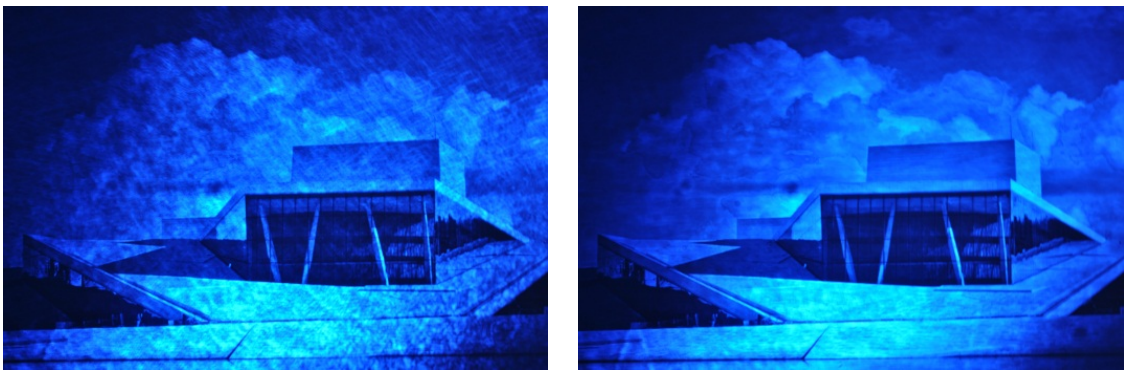

(a) (b)

Figure 2.12: Images from the projector without speckle suppression (a) and with speckle suppression (b)

## 2.2 MEMS diffuser for speckle suppression-Second generation

### 2.2.1 Motivation

The design, characterization and demonstration of first generation of MEMS diffuser for speckle suppression is presented in the section 2.1. It can be seen that the speckle reduction performance of our MEMS diffuser is not as good as achieved in [59]. There are two main reasons that affect the speckle suppression performance of the MEMS diffuser. Firstly, a diffuser that was used in [59] has continuous height profile while the MEMS diffuser has two-level binary height profile. For a reflected light, the phase fluctuation is wrapped in the interval $(0, 2\pi)$. Hence if the diffuser with continuous surface profile has large height fluctuations, the autocorrelation function of the reflected wave is narrower than the autocorrelation function of the surface height [38]. In such case, the coherence area of the reflected wave becomes much smaller than the correlation area of the random diffuser. However, in our case with a two-level binary diffuser, the auto-correlation area of the reflected wave is of similar size as that of the surface height, resulting in less speckle reduction as compared to the case when diffuser has continuous height profile.

Secondly, in the case of binary two-level random diffuser in the reflection geometry, if the height difference between the two levels is $\lambda/2$, the reflected wave phase profile becomes flat diffracting light only into zero order. The autocorrelation function of the reflected wave is no more a narrow-peaked function but significantly broadens, making it inefficient for speckle reduction. Thus, the difference in height of the two levels of the random diffuser should be optimized in order to have high speckle reduction efficiency. However, the surface height variations profile of the random pattern is limited by the fabrication process of MEMSCAP which is $500nm$ of height difference.

For further investigation of speckle suppression by MEMS diffuser with random patterns, a new generation of MEMS diffuser device is designed. In the new generation of MEMS diffuser device, the height difference of the two levels random patterns is increased for reduced surface roughness correlation length of the diffuser.

### 2.2.2 Design

There are two different designs for the second generation of MEMS diffuser device. The first design which is noted as "design $A$" has the same structure as of the first generation MEMS diffuser device. The largest diffuser displacement of this design is $75\mu m$. For further speckle suppression efficiency, another design which is named as "design $B$" is modified to have displacement up to $150\mu m$. In order to attain large displacement of the diffuser, the design of the springs is changed. The simulation of springs at largest displacement of both designs are shown in Figure 2.13. As shown in Figure 2.13 (b), dummy structure is added to the springs design to avoid over etching during fabrication process due to large opening area.

### 2.2.3 Characterization

The devices are fabricated by SINTEF based on MEMS process on SOI wafer. The wafer has $2\mu m$ of buried oxide (BOX) layer and $25\mu m$ thickness of the device layer. In the first generation of MEMS diffuser, the random patterns are formed on top of the moving mass by two metal deposition steps. In the second generation of MEMS

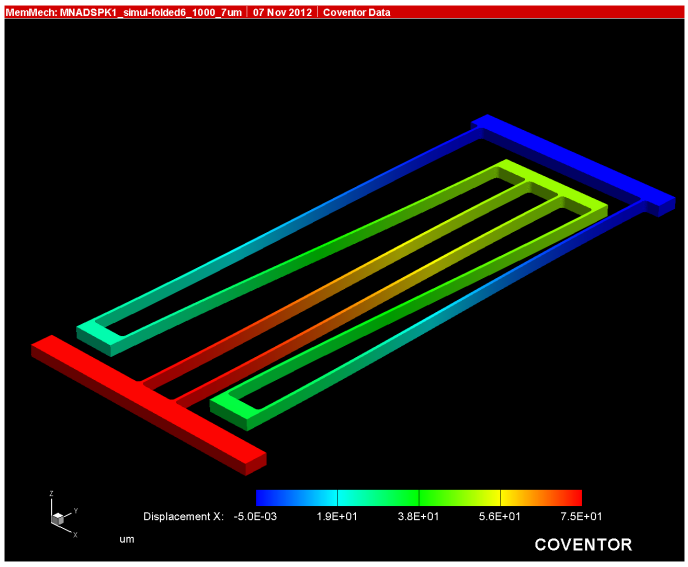


(a)

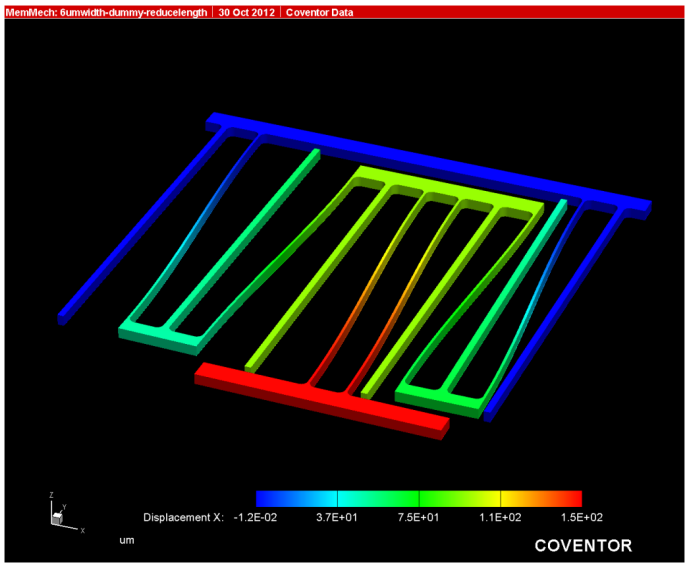


(b)

Figure 2.13: Spring design at maximum displacement for design $A$ (a) and for design $B$ (b)

diffuser, the random patterns are generated by the reactive ion etching (RIE) directly to the surface of device layer. In the final step of fabrication process, a 100nm layer of Aluminum is deposited all over the device for optical reflection. An image of the MEMS diffuser device of the design $A$ from the top view is shown in Figure 2.14 (a) and a closed up spring image of the design $B$ is shown in Figure 2.14 (b).

Figure 2.15 (a) shows the top view of the random patterns that have thickness about $3.6\mu m$. A continuous surface is expected for better speckle suppression. Therefore, a sidewall of random pattern is plotted for both first generation and second generation of MEMS diffusers for comparison. The side wall slope angle $\alpha$ as shown in the Figure

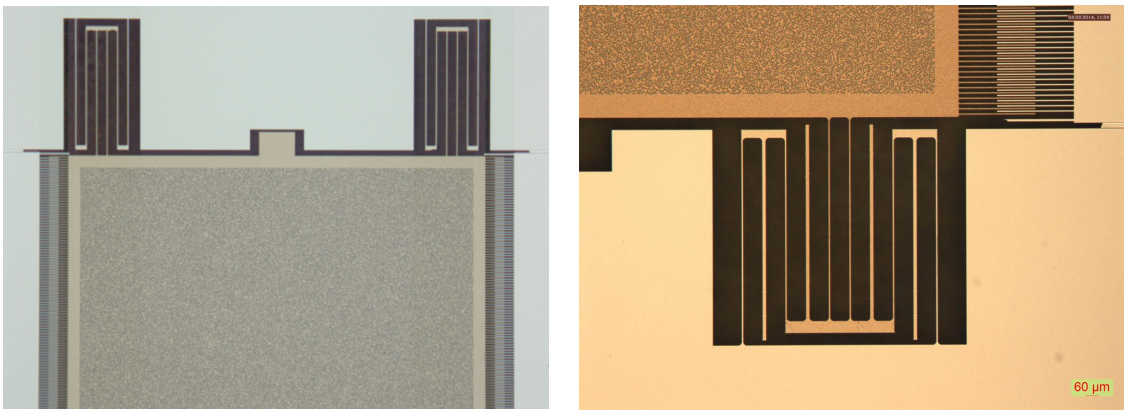


(a) (b)

Figure 2.14: Topview images of MEMS diffuser design $A$ (a) and spring of the design $B$ (b)

2.15 (b) is used for the comparison. The side wall slope angle of first generation MEMS diffuser device $\alpha$ is $18.7^o$ while this angle of second MEMS diffuser device is $9.3^o$. It can be concluded that the vertical side wall random patterns of the second generation MEMS diffuser is steeper than that of the first generation.

The stroboscopic method is used to determine the resonance frequencies of the two designs. The dynamic characterization is done for two devices of the design $A$ and one device of the design $B$. Since the design $A$ has the same structure as of the first generation of the MEMS diffuser, it is expected to have the same resonance frequency as the first generation of the MEMS diffuser. As shown in Figure 2.16 (a), the two devices of the design $A$ have resonance frequencies of 289.4Hz and 289.8Hz. This value is slightly lower than the resonance frequency of the first generation of MEMS diffuser which is 298.1Hz. The difference of resonance frequency can be explained by the difference of spring stiffness. The two generations of MEMS diffuser devices are fabricated by two different processes. The different parameters in the RIE process causes different over etch of the spring beam. This leads to the change of spring stiffness and causes the difference in resonance frequency. Another reason causes the change in spring stiffness is the stress of the metal layer. For the second generation, an Aluminum layer is deposited on the whole device for optical reflection. The high temperature of the deposition process caused the stress in the metal layer. This internal stress may cause a small change on the spring stiffness. The difference in displacement amplitude of the two generations is a result of different applied voltage. For the first generation, the device is measured by applying 5V DC bias and 10V

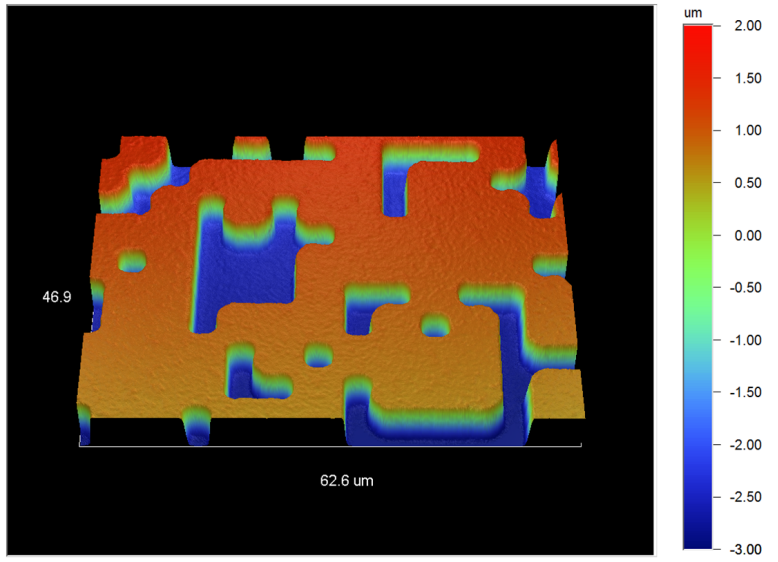


(a)

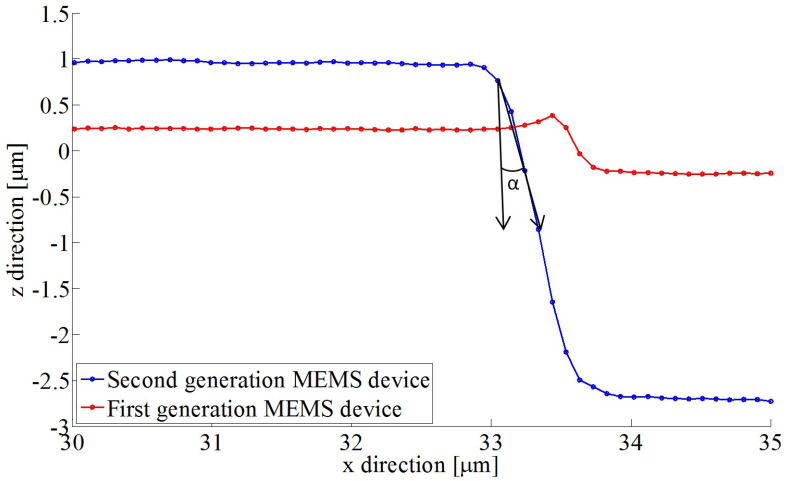


(b)

Figure 2.15: Random surface patterns of second generation MEMS diffuser (a) and side wall of the first and second generation MEMS diffuser (b)

AC bias while 4V DC bias and 10V AC bias of driving voltage are used for the measurement of second generation MEMS diffuser.

Figure 2.16 (b) shows the resonance frequency of the design $B$. The device exhibits resonance frequency at 359.1Hz. Only small voltage is applied to the device. At high driving voltage, the movement of the diffuser is no longer dominated by in-plane movement but the out of plane movement appears. The out of plane movement causes the stiction of the comb fingers as shown in Figure 2.17 and this leads to short circuit. The diffuser can not move any more.

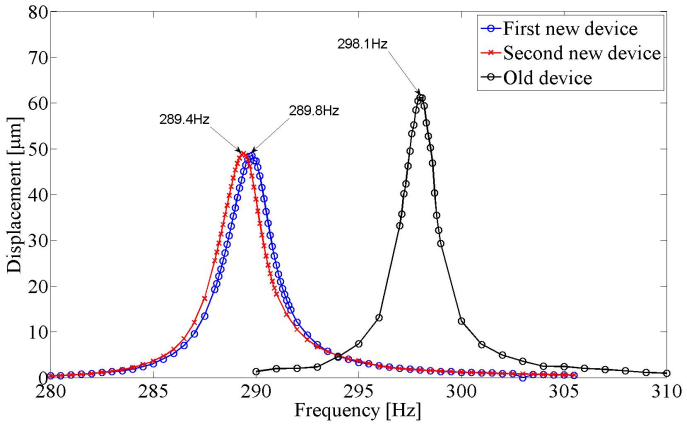


(a)

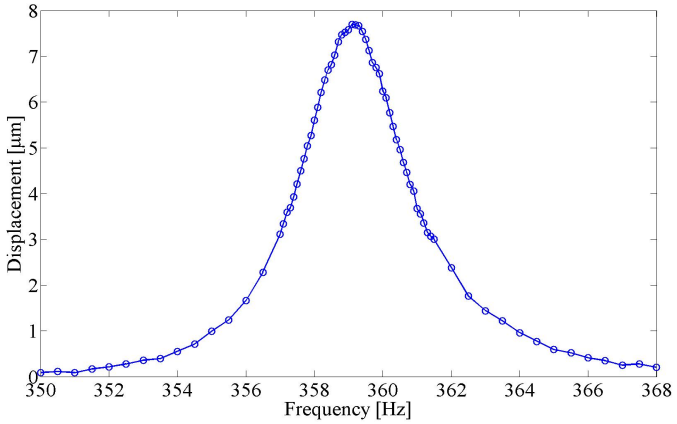


(b)

Figure 2.16: Resonance frequency of the design $A$ (a) and of the design $B$ (b)

### 2.2.4 Speckle contrast suppression characterization

As a large displacement of diffuser can not be attained by the design $B$ because of stiction problem. Only the design $A$ is used for speckle suppression characterization. Freespace geometry is used for speckle measurement. The device is driven at resonance frequency and speckle images are captured with different displacement amplitude which is controlled by applied voltage. Speckle contrast measurement for the first and the second generation of MEMS diffuser are both plotted in Figure 2.18. Because the second generation of MEMS diffuser is driven at resonance frequency so smaller value of applied voltage is need to attain the maximum displacement. By varying the applied voltage from 0V to 11V, speckle contrast reduces from 0.791 to 0.545 for the second generation of MEMS diffuser. This corresponds to 31% of speckle contrast is reduced while up to 43% of speckle contrast reduction is achieved for the first generation of MEMS diffuser. Lower speckle suppression efficiency of

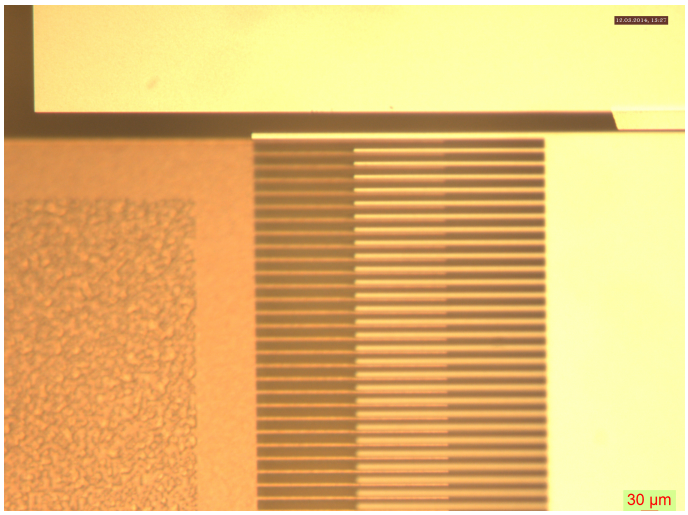


Figure 2.17: Stiction of comb fingers of the design B at high driving voltage

the second generation MEMS diffuser is possibly caused by the less side wall slope of random patterns of the second gerenation of MEMS diffuser.

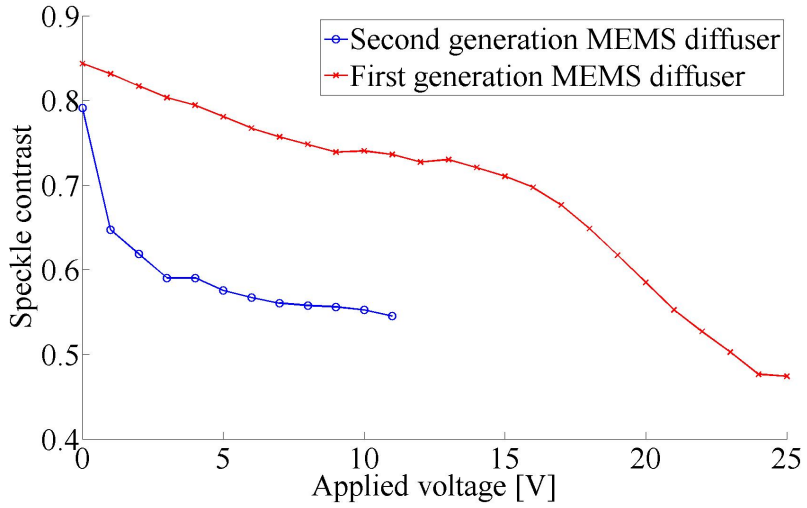


Figure 2.18: Speckle contrast measurement with the change of applied bias

## 2.3 Deformable mirror for speckle suppression

### 2.3.1 Introduction

A commercial phase-randomizing deformable mirror for anti-speckle technology was used for the study [66]. It comprises of a continuous surface of mirrors array that can be individually deformed and actuated up to hundreds of kHz. Inactive deformable mirror is shown in Figure 2.19 (a). The mirror is coated with Silflex for high op-

tical reflection efficiency over the range of visible wavelengths. When the mirror is activated, the coming light beam is reflected with maximum divergence angle of $2^o$. Figure 2.19 (b) shows deformable mirror in active with randomly distributed surface deformation. Due to the randomly distributed deformation at high frequency, many uncorrelated speckle patterns are produced. Thus, the speckle contrast of the projected image is reduced.

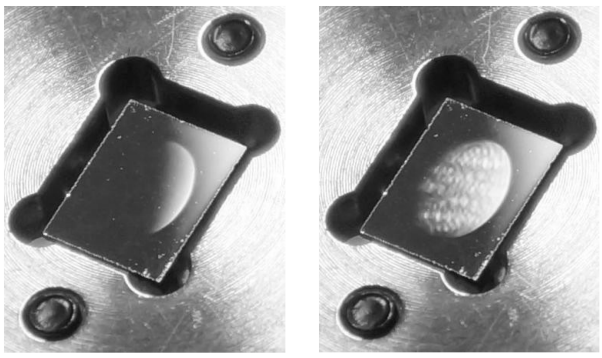

(a) (b)

Figure 2.19: Deformable mirror with elliptical active area, deformable mirror inactive (a) and deformable active (b) [66]

### 2.3.2 Speckle characterization for single laser

## Journal paper 2

#### Experimental results

The experiment is setup as shown in Figure 2.20. The laser is driven in continuous mode at fixed temperature of $25^oC$. An absorptive neutral density filter is used to attenuate the transmittance light so that it does not saturate the CCD camera. The initial laser beam is then split into two equivalent intensity beams by a non-polarizing beam splitter. The reflected beam is steered to a spectrometer and the transmitted beam is extended by a lens before propagating to the deformable mirror to avoid the damage of the mirror by high power density. The reflected beam from the mirror is focused and imaged on to the first diffuser. The scattered laser beam passed through a light pipe which has a second diffuser placed at the output face of the light pipe for beam homogenization. The measurement is done with two setups

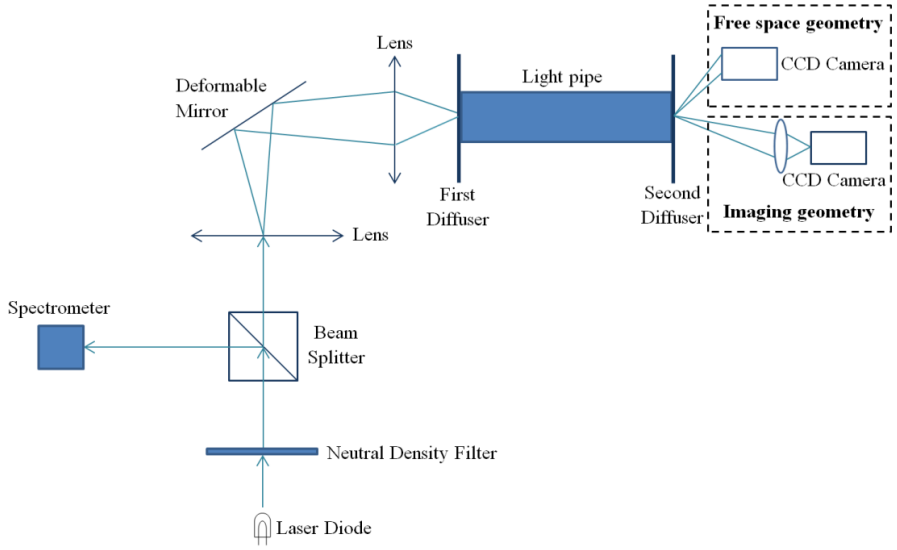


Figure 2.20: Experiment setup

of the camera. For free space geometry, the camera without imaging lens is used to capture the speckle images. For imaging geometry, the camera is equipped with an imaging lens that has focal length $f$ of 50mm and fixed aperture number $F\#$.

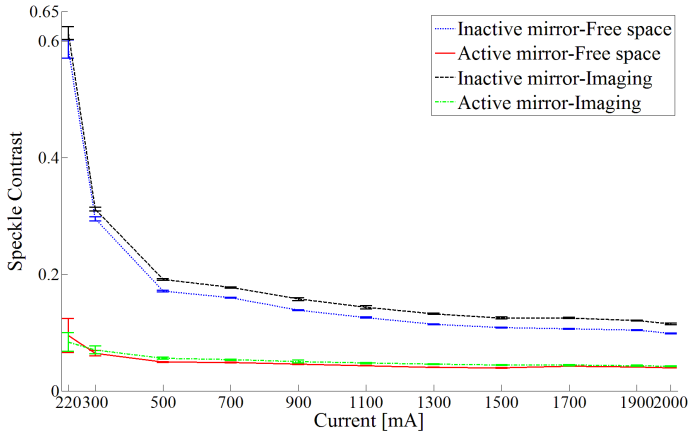


Figure 2.21: Speckle contrast measurement for blue Nichia NUB802T laser

The measurement is done for red and blue semiconductor laser diodes with a relative broad emission spectrum. The blue laser diode is the Nichia NUB802T laser with output power of 2.3W at current of 2A. The speckle contrast is measured by varying the driving current. A plot of measured speckle contrast for the blue laser with the change of driving current from 220mA to 2A is shown in Figure 2.21. The free space and imaging geometries setups show a small difference in speckle contrast values. When the mirror is inactivated, speckle contrast values change from 0.586 to 0.099 for free space geometry and from 0.614 to 0.115 for imaging geometry. It can be seen that speckle contrast reduces efficiently with the increase of driving current.

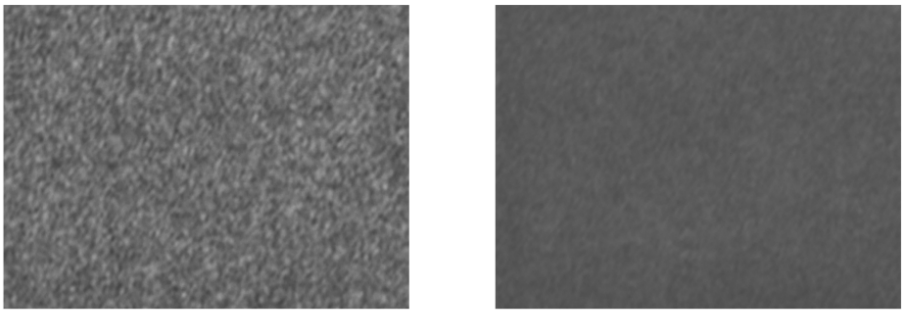


Figure 2.22: Speckle images of the blue laser for imaging geometry at driving current of $2A$ with inactive mirror (a) and with active mirror (b)

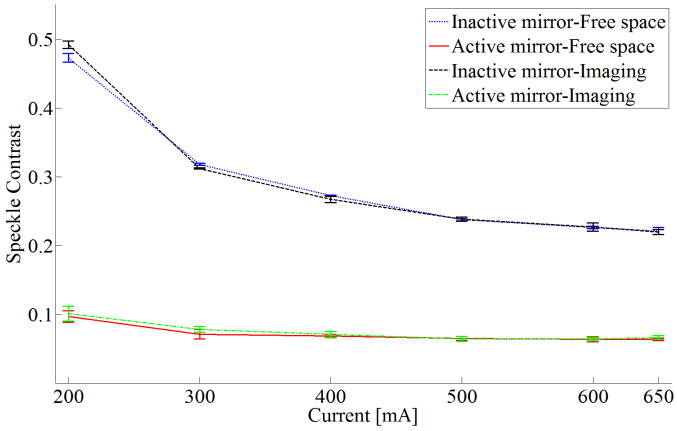


Figure 2.23: Speckle contrast measurement for red ML501P73 laser

The activation of the mirror introduces a good speckle reduction. When the mirror is activated, speckle contrast drops down to 0.095 for the free space geometry and to 0.084 for the imaging geometry at the driving current of 220mA. At $2A$ of driving current, the speckle contrast value is 0.04 for both geometry setups. The images of speckle with inactive mirror for the imaging geometry at current 2A are shown in Figure 2.22 (a). When the mirror is activated, speckle is reduced as shown in Figure 2.22 (b).

A red broad area laser Mitsubishi ML501P73 is used for the experiment. The laser provides $0.5W$ CW of output power at $650mA$. A separate collimating lens with focal length of $3.3mm$ is used to make the laser beam parallel. Speckle contrast measurement with the change of driving current from $200mA$ to $650mA$ for the red laser is plotted in Figure 2.23. With inactive mirror, speckle contrast reduces from 0.473 to 0.221 for free space geometry and from 0.492 to 0.22 for imaging geometry. With the active mirror at $200mA$ drive current, speckle contrast for free space and imaging geometries are 0.097 and 0.101. At driving current of $650mA$, the speckle

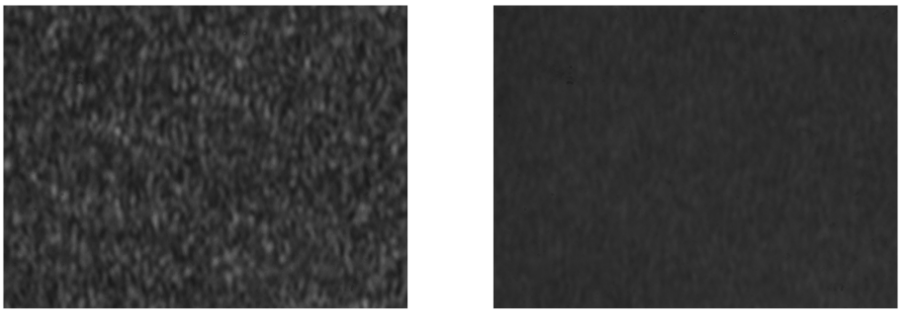


Figure 2.24: Speckle images of the red laser for imaging geometry at driving current of 650mA with inactive mirror (a) and with active mirror (b)

contrast is 0.063 for free space geometry and 0.066 for imaging geometry. Speckle images for the imaging geometry at driving current $650mA$ are shown in Figure 2.24. It can be seen that there is speckle reduction with active mirror Figure 2.24 (b) compare to speckle image with inactive mirror Figure 2.24 (a).

**Discussion**

Speckle is reduced by introducing independent speckle patterns $N$. For analysis, a reduction factor is defined as

$$R = \sqrt{N} \tag{2.4}$$

In this experiment, three different mechanisms for speckle reduction have been applied. The first method is the polarization diversity which gives polarization reduction factor $R_\sigma$. The second method of speckle reduction is the angle diversity $R_\Omega$ which is provided by the deformable mirror. Finally is the wavelength diversity method $R_\lambda$ which is given by the spectrum widening of the lasers. The maximum speckle reduction factor for the system is

$$R = R_\sigma R_\Omega R_\lambda \tag{2.5}$$

***Speckle suppression by the polarization diversity***

The diffusers scatter the light in the two orthogonal polarizations. The amount of speckle reduction depends on the degree of polarization of the light in the speckle patterns. For a fully depolarized speckle, the degree of freedom that is achieved by the polarization diversity is $N_\sigma = 2$. Therefore, an automatic $\sqrt{2}$ factor of of speckle reduction is obtained. The polarization reduction factor $R_\sigma$ of the polarization diversity can be determined from the experimental results in term of the speckle contrast at the threshold current when the mirror is inactive $C_{Imin}$

$$R_\sigma = \frac{1}{C_{Imin}} \tag{2.6}$$

Because speckle contrast value between free space and imaging geometries is small, only speckle contrast for free space geometry is used for the calculation. The calculation result is shown in the Table 2.3. The polarization speckle reduction factor $R_\sigma$ is $\sqrt{2.9}$ for the blue laser and $\sqrt{4.5}$ for the red laser. These values are higher than the theoretical value which is $R_\sigma = \sqrt{2}$. The reason for this is the lasers do have some spectrum width broadening even at the minimum driving current. The minimum driving current is slightly higher than the threshold current. Therefore, a number of independent speckle patterns are introduced by the wavelength diversity due to the finite spectrum width of the laser.

Table 2.3: Calculation of speckle reduction factors $R$ for free space geometry

| Speckle reduction factor | Blue laser | Red laser |
|---|---|---|
| $R_\sigma$ | $\sqrt{2.9}$ | $\sqrt{4.5}$ |
| $R_{\Omega_{min}} = \frac{C_{Imin}}{C_{Amin}}$ | 6.2 | 4.9 |
| $R_{\Omega_{max}} = \frac{C_{Imax}}{C_{Amax}}$ | 2.5 | 3.5 |
| $R_{\lambda_{inactive}} = \frac{C_{Imin}}{C_{Imax}}$ | 6 | 2.1 |
| $R_{\lambda_{active}} = \frac{C_{Amin}}{C_{Amax}}$ | 2.4 | 1.5 |

***Speckle suppression by the angle diversity with the deformable mirror***

Speckle contrast is reduced by the generation of time varying phase patterns which will effectively destroy the spatial coherence. The speckle reduction factor by the

angle diversity is the ratio between of speckle contrast when the deformable mirror is inactive $C_I$ and active $C_A$ at the same driving current

$$R_\Omega = \frac{C_I}{C_A} \tag{2.7}$$

As shown in the Table 2.3, the speckle reduction factor at minimum driving current is $R_{\Omega min} = 6.2$ and at maximum driving current is $R_{\Omega max} = 2.5$ for the blue laser. For the red laser, speckle reduction factor at minimum driving current is $R_{\Omega min} = 4.9$ and at maximum driving current is $R_{\Omega max} = 3.5$. It can be seen that there is difference in speckle reduction factor by angle diversity at maximum current and minimum current for the blue and the red lasers. The mirror provides a higher $R_\Omega$ at low current than at high current.

***Speckle suppression by the wavelength diversity***

Speckle contrast depends on the spectral bandwidth of the illuminating light source. For a broadband laser, more modes are excited in the laser at higher driving current. These different modes propagate independently and therefore cause the incoherence of the laser beam. Due to the incoherence of the laser beam at the high current driving regime, the speckle contrast is reduced as shown in the experiment. Speckle contrast is calculated in terms of spectrum bandwidth as

$$C = \left[1 + 2\pi^2 (n-1)^2 \left(\frac{\delta\nu}{\bar{\nu}}\right)^2 \left(\frac{\sigma_h}{\bar{\lambda}}\right)^2\right]^{-\frac{1}{4}} \tag{2.8}$$

where $\bar{\lambda}$ is the central wavelength, $\bar{\nu}$ is the negative of the center frequency, $n$ and $\sigma_h$ are the refractive index and the root mean square surface roughness of the diffusers.

The speckle reduction factor by the wavelength diversity is expressed as

$$R_\lambda = \frac{C_{min}}{C_{max}} \tag{2.9}$$

By adjusting the driving current from the threshold to the maximum, the speckle

reduction factor with the inactive mirror $R_{\lambda inactive} = 6$ is estimated for the blue laser. When the mirror is active, the speckle reduction factor by wavelength diversity $R_{\lambda active}$ goes down to 2.4. Lower speckle reduction factor $R_\lambda$ is achieved by the red laser. The values of speckle reduction factor for the red laser are $R_{\lambda inactive} = 2.1$ with the inactive mirror and $R_{\lambda active} = 1.5$ with the active mirror.

It can be seen that better speckle contrast suppression by wavelength diversity is achieved by the blue laser. Since the blue laser has higher power than the red laser and it can be driven at higher current than the red laser. More modes are excited in the blue laser at high current and this leads to the more broaden of the spectrum. The Equation 2.8 indicates that the wider spectrum width $\delta\nu$, the lower of speckle contrast value is. A plot of the spectrum width at 20% of the maximum light intensity for the blue and the red laser with the logarithm scale current is shown in Figure 2.25. The spectrum width changes from $0.2nm$ at $220mA$ to $2.02nm$ at $2A$ of driving current for the blue laser. The spectrum width of the red laser at $200mA$ driving current is $0.665nm$ and the spectrum width is $1.06nm$ at maximum driving current $650mA$.

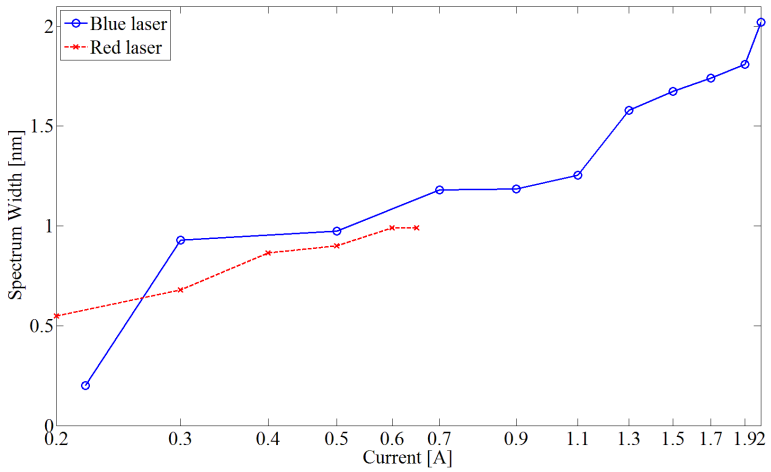


Figure 2.25: Spectrum of the blue laser Nichia NUB802T and of the red laser ML501P73

### 2.3.3 Speckle characterization for laser array

## Draft of Journal paper 3

Speckle suppression by the deformable mirror characterization is also done for laser array. Different number of lasers and different types of lasers are used for the investigation. The experiment setup is the same as shown in Figure 2.20 but only free space geometry is used for the measurement.

**Experimental results**

The blue laser Nichia NUB802T is used for the measurement. The laser has optical output power of $2.3W$ at $2000mA$ driving current. The dominant central wavelength of this laser at $2000mA$ driving current is from $455nm$ to $470nm$. Speckle contrast is measured at different driving currents for one and two lasers as shown in Figure 2.26. When the mirror is inactivate, the speckle contrast values are 0.641 and 0.304 for one laser and two lasers respectively at the minimum driving current. Speckle contrast reduces with the increase of driving current. At $2000mA$ driving current, the speckle contrast is 0.119 for one laser and 0.098 for two lasers. Speckle contrast is further reduced by the active mirror by adding extra degree of freedom through angle diversity. For one laser, speckle contrast is 0.126 at $220mA$ and 0.04 at $2000mA$ when the mirror is active. Speckle contrast is 0.044 at $250mA$ and 0.033 at $2000mA$ for the two lasers with the active mirror.

The same measurement is done for another type of blue laser Nichia NUB801E. This laser has higher threshold current. At $2300mA$ driving current, the laser has power of $3.4W$ and the central wavelength is from $440nm$ to $455nm$. The result is plotted in Figure 2.27. When the mirror is inactive, the speckle contrast is 0.46 at $280mA$ for one laser. This value reduces to 0.115 at $2000mA$. For the two lasers with inactive mirror, the speckle contrast is 0.15 at $300mA$ and 0.066 at $2000mA$. When the mirror is activated, speckle contrast is 0.055 at $280mA$ for one laser and 0.045 at $300mA$ for two lasers. At $2000mA$ of driving current, the speckle contrast value is the same for both cases 0.035.

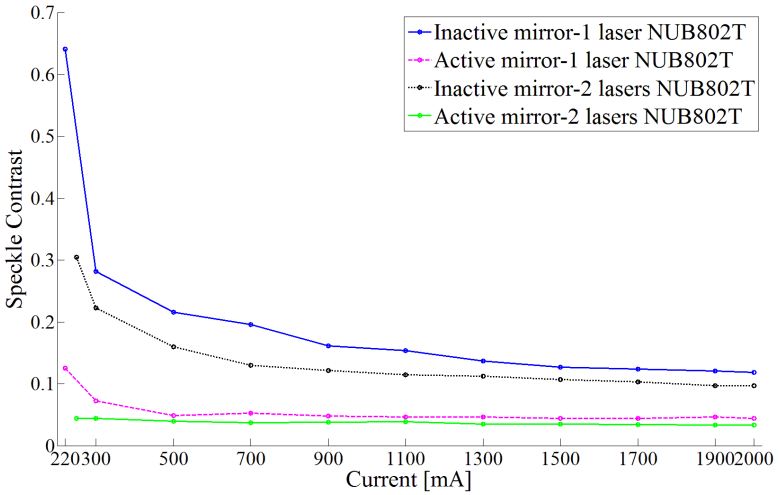


Figure 2.26: Speckle contrast measurement for one laser and two lasers NUB802T

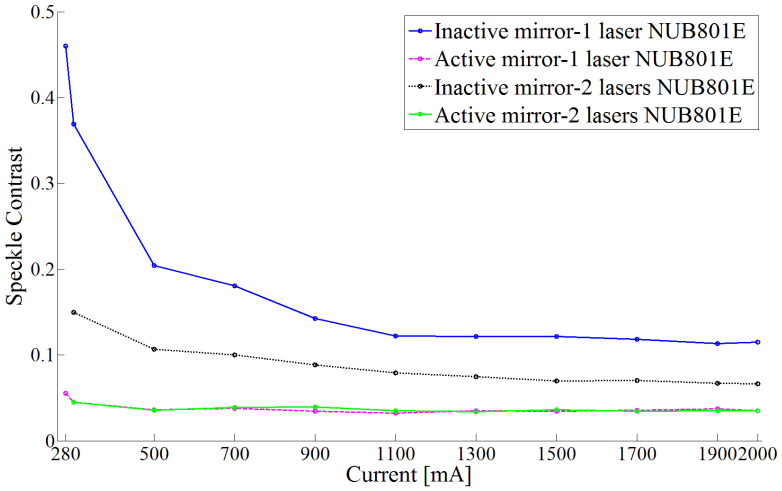


Figure 2.27: Speckle contrast measurement for one laser and two lasers NUB801E

The measurement is repeated for the four lasers setup. Two different setups of the lasers are used for the measurement. The first setup is four lasers NUB802T and the second setup is a combination of two lasers NUB802T and two lasers NUB801E. The results are plotted in Figure 2.28. When the mirror is inactive, the speckle contrast is 0.225 at $250mA$ and it reduces to 0.06 at $2000mA$ for four lasers NUB802T. In the case of two lasers NUB802T and two lasers NUB801E, speckle contrast with inactive mirror is 0.094 at $300mA$ and 0.045 at $2000mA$. When the mirror is active, speckle contrast is 0.045 there is a small difference in speckle contrast for both setups. Speckle contrast is 0.045 at $250mA$ for four lasers NUB802T and 0.04 at $300mA$ for the combination of two lasers NUB802T and two lasers NUB801E. The speckle contrast value is the same for the two setups which is 0.033 at $2000mA$ driving current.

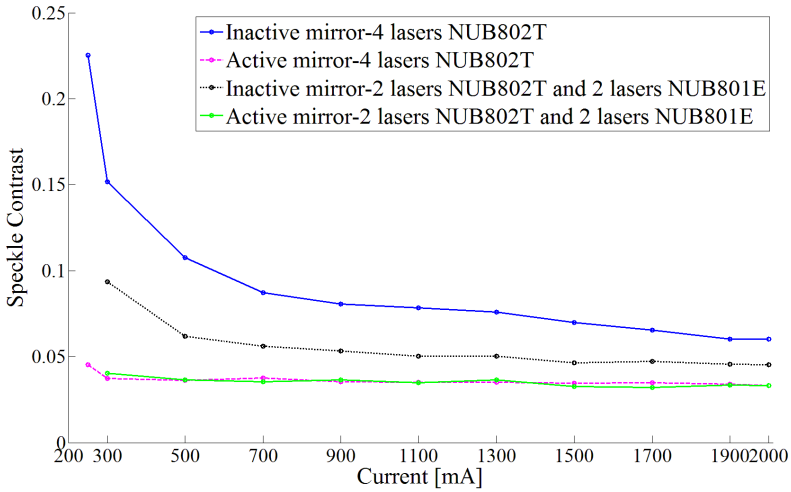


Figure 2.28: Speckle contrast measurement for four lasers NUB802T and combination of two lasers NUB802T and two lasers NUB801E

### Discussion

The main difference in speckle suppression of laser array and single laser as presented in the previous part is speckle suppression by wavelength diversity. Thus, only speckle suppression by wavelength diversity is discussed here. In this experiment, speckle contrast is reduced by spreading line widths of the laser light sources and by using different laser sources that have different central wavelengths. Figure 2.29 shows the laser spectrum for the two lasers setup with different driving current. It can be seen that the two independent laser sources have a slight difference in

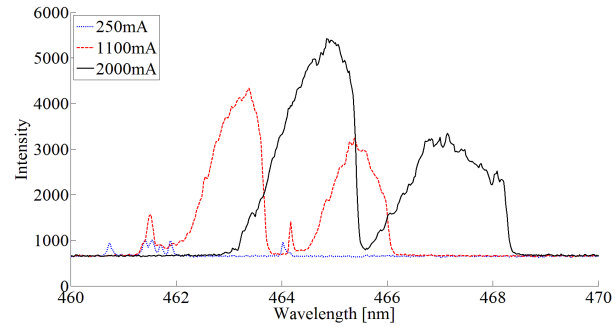


(a)

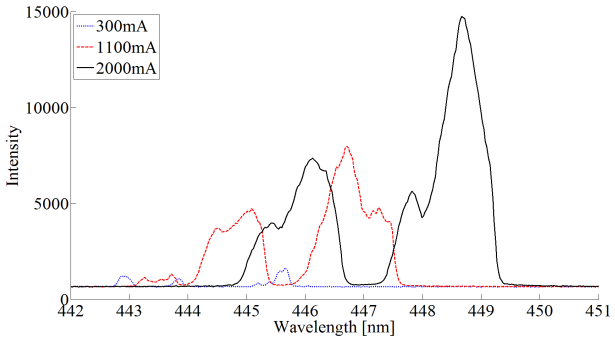


(b)

Figure 2.29: Spectrum of 2 lasers NUB802T (a) and spectrum of 2 lasers NUB801E (b) with the change of driving current

their central wavelengths. As the driving current increases, the central wavelength of the lasers shifts towards longer wavelength and the spectrum becomes wider. The plot of laser spectrum width at 20% of maximum light intensity for one and two lasers is shown in Figure 2.30. For one laser NUB802T, the spectrum width is $0.2nm$ at minimum driving current $220mA$ and it goes up to $2.02nm$ at $2000mA$ of driving current. At minimum driving current $280mA$, the spectrum width of one laser NUB801E is $0.36nm$. At $2000mA$ driving current, the width of the spectrum is $1.69nm$. The laser spectrum is even broader with two lasers. The spectrum width is $0.86nm$ for two lasers NUB802T at $250mA$ driving current while this value is $4.27nm$ at $2000mA$ driving current. For two lasers NUB801E, the width of the spectrum changes from $1.02nm$ to $3.23nm$ when the driving current increases from $300mA$ to $2000mA$. The introducing of broader spectrum of the two lasers explains the better speckle suppression by wavelength diversity.

Wider spectrum of lasers can be attained with the four lasers and therefore speckle contrast is further reduced. A plot of calculated spectrum width is shown in Figure 2.31. For the four lasers NUB802T, the spectrum width is $1.15nm$ at $250mA$ and

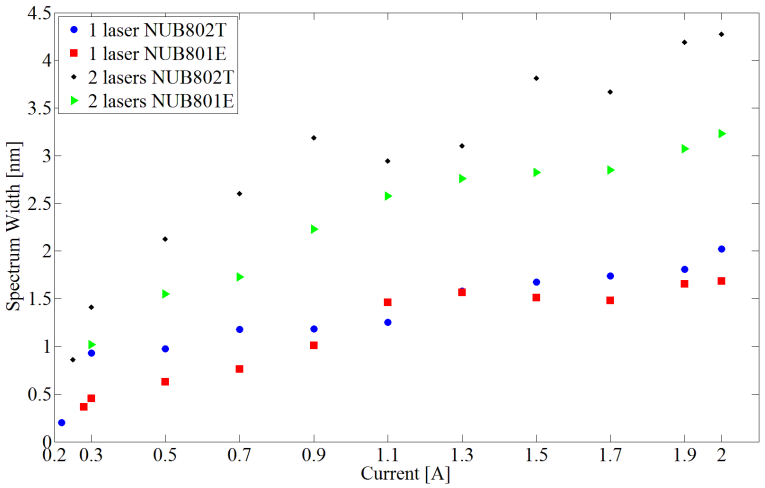


Figure 2.30: Total spectrum width of one and two lasers at 20% maximum light intensity

4.82$nm$ at 2000$mA$ driving current. Four lasers with two different types of laser can provide better speckle contrast reduction. The broader of laser spectrum is one of the reasons for better speckle contrast reduction in this case. At 250$mA$ driving current, 1.25$nm$ of spectrum width is introduced by the combination of two lasers NUB802T and two lasers NUB801E. It can be seen that the difference in spectrum width between the two cases of four lasers is small at low driving current. The difference of spectrum width is bigger at high driving current. The spectrum width is up to 6.73$nm$ at 2000$mA$ for the two lasers NUB802T and two lasers NUB801E setup.

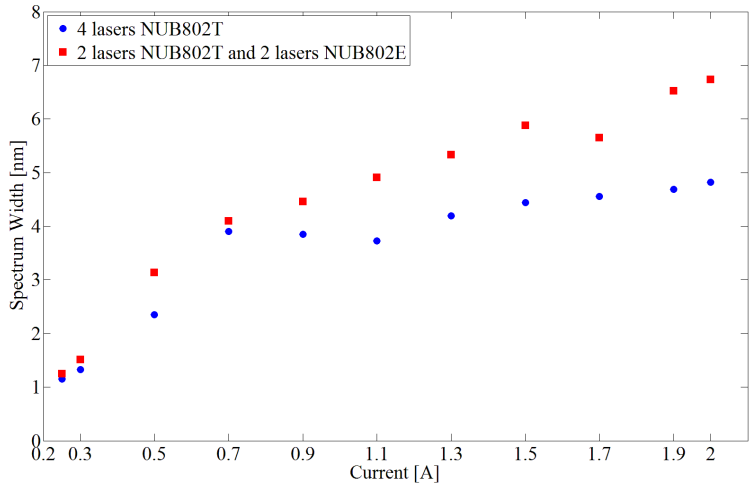


Figure 2.31: Total spectrum width of four lasers NUB802T and two lasers NUB802T and two lasers NUB801E at 20% maximum light intensity

In addition, the correlation of speckle patterns is an another reason that the com-

bination of two lasers NUB802T and two lasers NUB801E provides better speckle contrast reduction compare to the four lasers NUB802T. The speckle patterns from two independent light sources that have lasing wavelength at $\lambda_1$ and $\lambda_2$ become independent to each other only when the difference in wavelength of the light sources satisfies

$$\Delta\lambda \geq \frac{\bar{\lambda}^2}{(n-1)\,\sigma_h} \tag{2.10}$$

where $\Delta\lambda = |\lambda_2 - \lambda_1|$ is the wavelength difference of the two beams, $\bar{\lambda} = (\lambda_1 + \lambda_2)/2$ is the average wavelength and $\sigma_h$ is the standard deviation of surface roughness. Figure 2.32 shows spectrum of four lasers NUB802T and spectrum of the combination of two lasers NUB802T and two lasers NUB801E at 2000mA driving current. It can be seen that the spectrum of four lasers NUB802T are added up together. Consequently, the condition to achieve uncorrelated speckle patterns is not fulfilled. Thus, the speckle contrast reduction of four lasers of the same type NUB802T is not as good as the speckle contrast reduction of the combination of two lasers NUB802T and two lasers NUB801E.

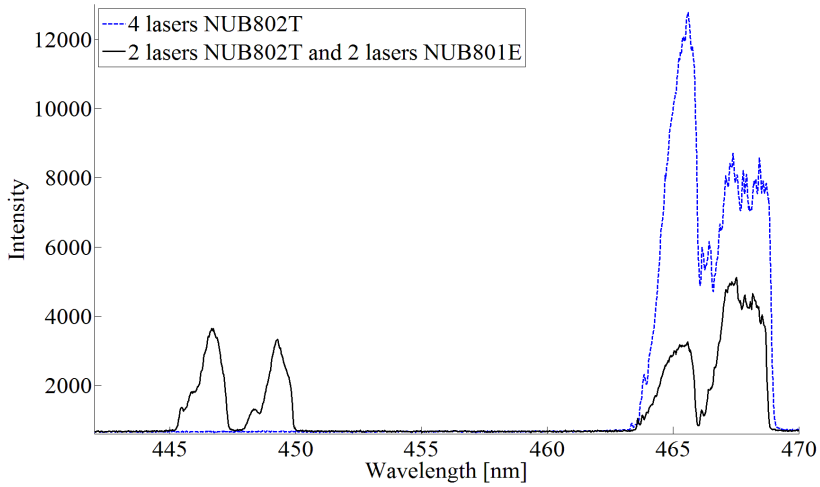


Figure 2.32: Spectrum distribution of 4 lasers NUB802T and 2 lasers of NUB802T and 2 lasers of NUB801E at 2000mA of driving current

## 2.4 Application and characterization of speckle suppression methods in laser projection system

### Conference paper 4

A laser projection system platform is built at Projectiondesign AS. The hybrid solution which is a combination of lasers and Phosphor is chosen for the laser projection system. Because of the high price of the green lasers, Phosphor is used to generate the green light by the use of blue lasers as an excitation source. The system consists of 6 blue laser banks from Nichia (each laser bank has 8 individual laser diodes), 74 red lasers from Mitsubishi, and 8 blue laser banks from Nichia for Phosphor excitation source. Each blue laser bank has an output power of 30W while each red laser has an output power of 0.5W in continuous driving. Figure 2.33 shows simulation of laser beam with optical system of the projection system by Zemax. This is a single DMD chip projection system which can provide about 10 000 lumen. The projection system is shown in Figure 2.34 (a) and the system in running the red lasers is shown in Figure 2.34 (b).

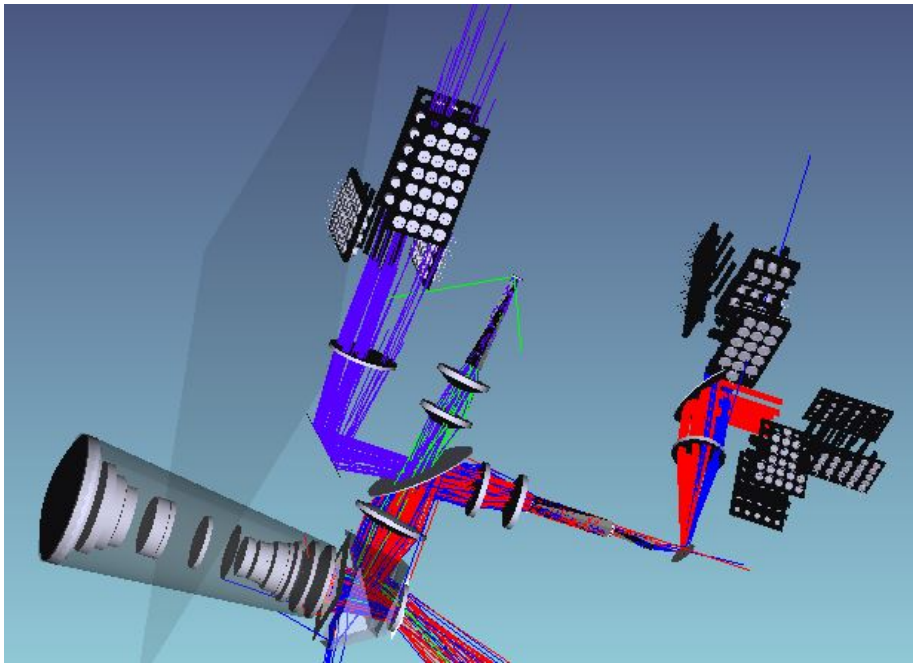

Figure 2.33: Zemax simulation of the laser/Phosphor projection system

Speckle contrast of the projection system is characterized. There are many methods for speckle suppression that are applied in the system. Each source in the array

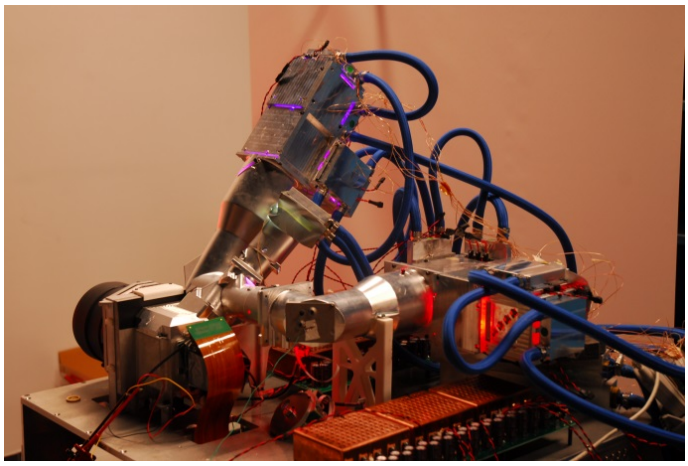

(a)

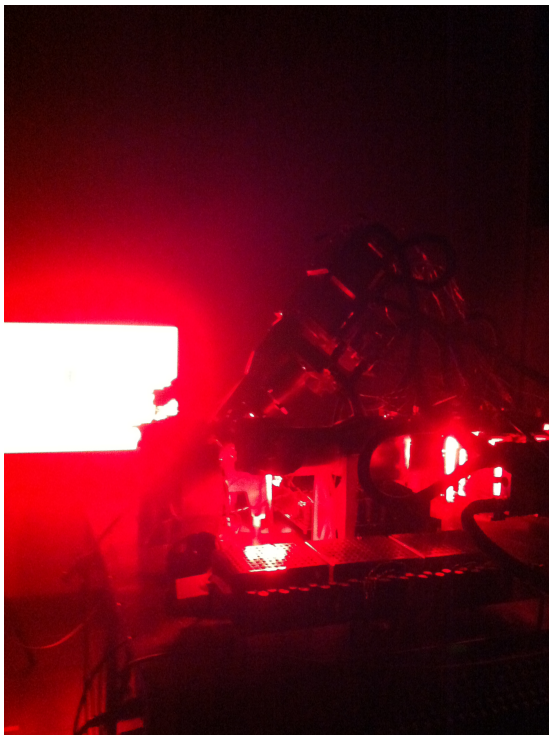

(b)

Figure 2.34: Laser projection system (a) and the system running in the red lasers (b)

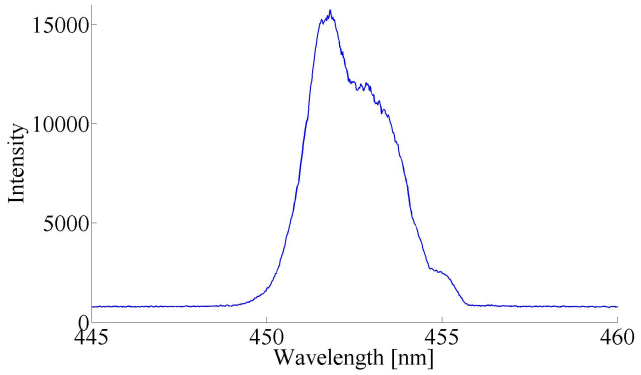


(a)

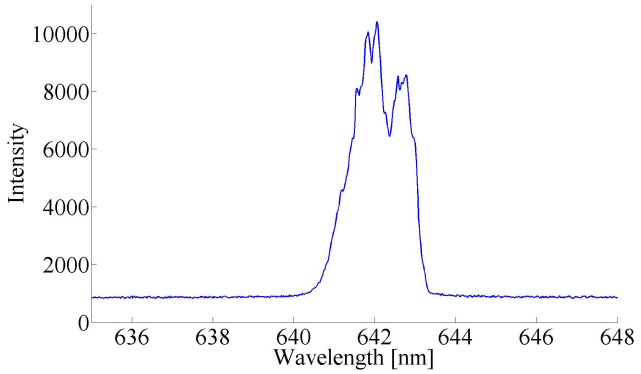


(b)

Figure 2.35: Spectrum of the blue lasers (a) and spectrum of the red lasers (b)

generates separate speckle patterns which add together. If the distance between the sources are large enough, these superimposed speckle patterns will be uncorrelated. Thus, speckle contrast is reduced due to the difference of the illumination angle. In the projection system, the distance between the lasers on the laser bank is $1cm$ to introduce speckle suppression by angle diversity. Angle diversity for speckle suppression is also achieved by the use of and optical elements that scatter light in the system.

Another method for speckle suppression in the projection system is wavelength diversity which is introduced by using a number of independent laser sources. The independent laser sources have a slight difference in wavelength themselves and this offers the broadening of the light source spectrum. Figure 2.35 shows the spectrum of blue and the red lasers array. Full width of half maximum spectrum bandwidth is $5nm$ for the blue lasers array and $2nm$ for the red lasers array.

A commercial moving diffuser is inserted into the system for further speckle suppression. The moving diffuser has diffusion angle of $4.2^o$. The diffuser has oscillation

frequency of 300Hz and the displacement amplitude is between $200\mu m - 300\mu m$. The measurement is done in the focus condition which means the camera is focused on the screen. Since the aperture number $F\#$ determines the average size of the speckles patterns in relation to the area of the camera pixels, the $F\#$ number matched to human pixel size to avoid spatial averaging is [67]

$$F\# = \sqrt{\frac{\pi A_p}{1.17\lambda^2}} \tag{2.11}$$

where $A_p$ is the camera pixel area and $\lambda$ is the wavelength of laser source. By matching the equation (2.11) to the clear aperture of the human visual system $3.2mm$, the focal length of imaging lens is

$$f = \sqrt{\frac{\left(3.2 \times 10^{-3}\right)^2 \pi A_p}{1.17\lambda^2}} \tag{2.12}$$

From the Figure 2.35, the central wavelengths at $452nm$ for the blue laser array and $642nm$ for the red laser array are used for the calculation of focal length and $F\#$ for the camera lens. The setup of the camera lens for the measurement is shown in Table 2.4. The focal length and $F\#$ of the lens are $35.9mm$ and 11.2 for the red laser. For the blue laser, these values are $51mm$ and 16.

Table 2.4: Focal length and Aperture number $F\#$ of the lens for the measurement

| Laser array | Central wavelength | Focal length | Aperture number $F\#$ |
|---|---|---|---|
| Red | $642nm$ | $35.9mm$ | 11.2 |
| Blue | $452nm$ | $51mm$ | 16 |

Speckle contrast is measured with the change of distance between the camera lens and the screen $d$. As shown in [67], speckle contrast decreases by a factor

$$\sqrt{N} = \sqrt{\frac{\Omega_{proj}}{\Omega_{det}}} \propto \sqrt{\frac{\Omega_{proj}}{D^2/d^2}} \tag{2.13}$$

where $\Omega_{proj}$ is the solid angle between the projector and the screen, $\Omega_{det}$ is the solid angle subtended by the entrance pupil of the detector to the screen and $D$ is the aperture of the camera.

The lasers are driven in pulse wave condition. The red lasers are driven at the current of $1A$ and the duty cycle is 33% while the blue lasers are driven at a current of $2.5A$ and the duty cycle is 25%. The speckle contrast suppression characterization result is shown in Table 2.5. Speckle contrast is measured at $25cm$, $60cm$ and $90cm$ distance $d$ from the screen to the camera lens. For the blue laser, speckle contrast is measured with the change of distance $d$ from $60cm$, $71cm$ and $140cm$ as can be seen in the Table 2.6. For both cases, speckle contrast reduces as the observed distance $d$ increases. This is in agreement with theory which is shown in Equation (2.13). Lower speckle contrast is attained by the activation of moving diffuser.

Table 2.5: Speckle suppression by moving diffuser for red lasers array

| Distance [cm] | Speckle contrast diffuser off | Speckle contrast diffuser on |
|---|---|---|
| 25 | 8.94% | 8.44% |
| 60 | 5.95% | 5.28% |
| 90 | 5.66% | 5.04% |

Table 2.6: Speckle suppression by moving diffuser for blue lasers array

| Distance [cm] | Speckle contrast diffuser off | Speckle contrast diffuser on |
|---|---|---|
| 60 | 11.87% | 11.47% |
| 71 | 11.18% | 11.03% |
| 140 | 5.19% | 3.87% |

# Chapter 3

# Conclusion and Future work

The main focus of this PhD work is the investigation, application and characterization of practical speckle suppression methods for laser projector. The first approach for speckle suppression is MEMS diffusers with random patterns on top of the moving mass for temporal averaging of speckle contrast. It is important that the movement of the diffuser has a pure sinusoidal in-plane motion to have extremely large degree of temporal diversity. Therefore, dynamic characterization is done for the determination of resonance frequencies and displacement waveform. From the experimental characterization, the MEMS diffuser performs sinusoidal displacement. Speckle contrast suppression is analyzed for both free space geometry and imaging geometry. The MEMS diffuser offers up to 43.8% and 26.8% of speckle suppression for free space and imaging geometries respectively. Speckle suppression by MEMS diffuser is also demonstrated in a commercial projector by using laser as a light source. The demonstration shows a significant speckle suppression of 34.8% on the projected images.

Speckle suppression of the first generation of MEMS diffuser performance is limited by the two-levels binary profile of the random patterns and the fix height difference of the two levels. The second generation of MEMS diffuser is designed and simulated to increase the height difference of random patterns with a continuous height profile. Dynamic and speckle suppression characterization are done. However, a continuous profile of random patterns can not be fabricated due to fabrication process properties. As a consequence, the second generation of MEMS diffuser does not perform

better speckle suppression than the first generation of MEMS diffuser.

Speckle contrast suppression of a commercial deformable mirror is studied with a combination of wavelength diversity by the use of single broadband lasers or laser array. The deformable mirror which consists of micro mirror array provides angle diversity to reduce speckle contrast. Low speckle contrast of 0.04 is attained for the single broadband laser by the combination of two methods. Lower speckle contrast value which is 0.033 is provided by the use of an array of broadband lasers. It is also shown experimentally that the use of lasers that have sufficient difference in wavelength offers better speckle suppression.

The practical application and characterization of speckle suppression methods in a laser projection system are performed. A various of methods for speckle suppression have been used in the laser projection system such as the use independent broadband lasers for wavelength diversity, distance between of the lasers for angle diversity and the use of moving diffuser for time varying speckle patterns generation. A very low speckle contrast projected images are attained by the combination of different methods for speckle suppression in the laser projection system.

Better speckle suppression by MEMS diffuser is possible by the optimization of fabrication process to attain a continuous surface of random patterns. In addition, the device can be redesigned to have larger area of moving mass so that the device can handle more power of the laser beam.

The use of more independent lasers in the projection system offers better speckle suppression by providing angle diversity and wavelength diversity. It is shown theoretically and experimentally that the lasing wavelength tends to shift toward the longer wavelength at high temperature. Thus, the lasers can be driven at different temperature to have broader bandwidth of lasers spectrum. The wavelength diversity can also be provided by using lasers that have slightly different central wavelength. High power lasers are required for high brightness projection system. Consequently, it is important for further investigation of speckle suppression module that can tolerate high optical power in the system.

# Bibliography

[1] Xing-Jie Yu, Y. L. Ho, L. Tan, Ho-Chi Huang, and Hoi-Sing Kwok. LED-based projection systems. *Journal of Display Technology*, 3(3):295–303, September 2007.

[2] Serdar Yeralan, Douglas Doughty, Rudi Blondia, and Rick Hamburger. Advantages of using high-pressure short-arc xenon lamps for display systems. volume 5740, pages 27–35, 2005.

[3] William T.Anderson and JR. Xenon compact arc lamps. *Journal of the Optical Society of America*, 41(6):385–387, 1951.

[4] Ulrich Weichmann, Jan W. Cromwijk, Gero Heusler, Uwe Mackens, Holger Moench, and Jens Pollmann-Retsch. Lightsources for small-etendue applications: a comparison of xenon and UHP lamps. volume 5740, pages 13–26, 2005.

[5] Koji Kawai and Masayuki Matsumoto. Short-arc metal halide lamp suitable for projector application. volume 2407, pages 23–35, 1995.

[6] Matthew S. Brennesholtz and Edward H. Stupp. *Projection Displays*. Wiley Publishing, 2nd edition, 2008.

[7] Guenther Derra, Holger Moench, Ernst Fischer, Hermann Giese, Ulrich Hechtfischer, Gero Heusler, Achim Koerber, Ulrich Niemann, Folke-Charlotte Noertemann, Pavel Pekarski, Jens Pollmann-Retsch, Arnd Ritz, and Ulrich Weichmann. UHP lamp systems for projection applications. *Journal of Physics D: Applied Physics*, 38(17):2995–3010, September 2005.

[8] Holger Moench. Optical modeling of UHP lamps. volume 4775, pages 36–45, 2002.

[9] Ulrich Weichmann, Hermann Giese, Ulrich Hechtfischer, Gero Heusler, Achim Koerber, Holger Moench, Folke-Charlotte Noertemann, Pavel Pekarski, Jens Pollmann-Retsch, and Arnd Ritz. UHP lamps for projection systems: getting always brighter, smaller, and even more colorful. volume 5289, pages 255–265, 2004.

[10] Gerard Harbers, Serge J. Bierhuizen, and Michael R. Krames. Performance of high power light emitting diodes in display illumination applications. *Journal of Display Technology*, 3(2):98–109, June 2007.

[11] Karl Beeson, Scott Zimmerman, William Livesay, Richard Ross, Chad Livesay, and Ken Livesay. 61.5: LED-based light-recycling light sources for projection displays. In *SID Symposium Digest of Technical Papers*, volume 37, pages 1823–1826. Wiley Online Library, 2006.

[12] N. Narendran and Y. Gu. Life of LED-based white light sources. *Journal of Display Technology*, 1(1):167–171, September 2005.

[13] Teruichi Watanabe, Kenji Nakamura, Shin Kawami, Yoshinori Fukuda, Taishi Tsuji, Takeo Wakimoto, and Satoshi Miyaguchi. Optimization of driving lifetime durability in organic LED devices using ir complex. volume 4105, pages 175–182, 2001.

[14] F. Fournier and J. Rolland. Design methodology for high brightness projectors. *Journal of Display Technology*, 4(1):86–91, March 2008.

[15] Ju-Nan Kuo, Hui-Wen Wu, and Gwo-Bin Lee. Optical projection display systems integrated with three-color-mixing waveguides and grating-light-valve devices. *Optics express*, 14(15):6844–6850, 2006.

[16] Matthijs H. Keuper, Gerard Harbers, and Steve Paolini. 26.1: RGB LED illuminator for pocket-sized projectors. In *SID Symposium Digest of Technical Papers*, volume 35, pages 943–945. Wiley Online Library, 2004.

[17] Denis Darmon, John R. McNeil, and Mark A. Handschy. 70.1: LED-illuminated pico projector architectures. In *SID Symposium Digest of Technical Papers*, volume 39, pages 1070–1073. Wiley Online Library, 2008.

[18] Chandrashekhar J. Joshi. 14.4 l: Late-news paper: Development of long life, full spectrum light source for projection display. In *SID Symposium Digest of Technical Papers*, volume 38, pages 959–961. Wiley Online Library, 2007.

[19] George Derderian and Robert J. Klaiber. *Laser beam deflector*. Google Patents, April 1969. US Patent 3,436,546.

[20] M. Jansen, G. P. Carey, R. Carico, R. Dato, A. M. Earman, M. J. Finander, G. Giaretta, S. Hallstein, H. Hofler, C. P. Kocot, S. Lim, J. Krueger, A. Mooradian, G. Niven, Y. Okuno, F. G. Patterson, A. Tandon, and A. Umbrasas. Visible laser sources for projection displays. volume 6489, pages 648908–648908–6, 2007.

[21] Hiroaki Sugiura, Tomohiro Sasagawa, Atsushi Michimori, Eiichi Toide, Takayuki Yanagisawa, Shuhei Yamamoto, Yoshihito Hirano, Masahiro Usui, Shigenori Teramatsu, and Jun Someya. 56.3: 65-inch, super slim, laser TV with newly developed laser light sources. *SID Symposium Digest of Technical Papers*, 39(1):854–857, May 2008.

[22] Greg Niven and Aram Mooradian. Trends in laser light sources for projection display. In *13th International Display Workshop (IDW 2006), Otsu, Japan*, 2006.

[23] Masamichi Sakamoto, Richard R. Craig, and John G. Endriz. Highly reliable high-power cw AlGaAs (808 nm) 1-cm bar laser diodes for nd:YAG pump application. volume 2379, pages 130–136, 1995.

[24] J. C. Brazas and M. W. Kowarz. High-resolution laser-projection display system using a grating electromechanical system (GEMS). In H. Urey and D. L. Dickensheets, editors, *MOEMS Display and Imaging Systems II*, volume 5348 of *Society of Photo-Optical Instrumentation Engineers (SPIE) Conference Series*, pages 65–75, January 2004.

[25] Wei-Feng Hsu, I.-L. Chu, and others. Speckle suppression by integrated sum of fully developed negatively correlated patterns in coherent imaging. *Progress In Electromagnetics Research B*, 34:1–13, 2011.

[26] Desmond C. Ong, Sanjeev Solanki, Xinan Liang, and Xuewu Xu. Analysis of laser speckle severity, granularity, and anisotropy using the power spectral density in polar-coordinate representation. *Optical Engineering*, 51(5):054301–1, 2012.

[27] L.J. Hornbeck. Digital light processing and MEMS: an overview. In *Advanced Applications of Lasers in Materials Processing/Broadband Optical Networks/Smart Pixels/Optical MEMs and Their Applications. IEEE/LEOS 1996 Summer Topical Meetings:*, pages 7–8, August 1996.

[28] Benjamin Lee. Introduction to digital micromirror device (DMD) technology. *Application Report of Texas Instruments*.

[29] Claude Tew, L. Hornbeck, Johnson Lin, Edison Chiu, Kevin Kornher, J. Conner, K. Komatsuzaki, and P. Urbanus. Electronic control of a digital micromirror device for projection displays. In *Solid-State Circuits Conference, 1994. Digest of Technical Papers. 41st ISSCC., 1994 IEEE International*, pages 130–131. IEEE, 1994.

[30] Gerard Harbers, Matthijs Keuper, and Steve Paolini. Performance of high power LED illuminators in color sequential projection displays. *Proc. of the 10th International Display Workshops, Paper LAD3-4*, 2003.

[31] Dmitri V. Kuksenkov, Rostislav V. Roussev, Shenping Li, William A. Wood, and Christopher M. Lynn. Multiple-wavelength synthetic green laser source for speckle reduction. pages 79170B–79170B–12, February 2011.

[32] Dmitri V. Kuksenkov, Rostislav V. Roussev, Shenping Li, William A. Wood, and Christopher M. Lynn. Multiple-wavelength synthetic green laser source for speckle reduction. pages 79170B–79170B–12, February 2011.

[33] Alexander Wong, Akshaya Mishra, Kostadinka Bizheva, and David A. Clausi.

General bayesian estimation for speckle noise reduction in optical coherence tomography retinal imagery. *Optics express*, 18(8):8338–8352, 2010.

[34] T. Mizushima, H. Furuya, K. Mizuuchi, T. Yokoyama, A. Morikawa, K. Kasazumi, T. Itoh, A. Kurozuka, K. Yamamoto, S. Kadowaki, and others. L-9: Late-news paper: Laser projection display with low electric consumption and wide color gamut by using efficient green SHG laser and new illumination optics. In *SID Symposium Digest of Technical Papers*, volume 37, pages 1681–1684. Wiley Online Library, 2006.

[35] A L Andreev, I N Kompanets, M V Minchenko, E P Pozhidaev, and T B Andreeva. Speckle suppression using a liquid-crystal cell. *Quantum Electronics*, 38(12):1166–1170, December 2008.

[36] Brandon Redding, Graham Allen, Eric Dufresne, and Hui Cao. Low-loss high-speed speckle reduction using a colloidal dispersion. In *CLEO: 2013*, OSA Technical Digest (online), page JW2A.66. Optical Society of America, June 2013.

[37] Chien-Yue Chen, Wei-Chia Su, Ching-Huang Lin, Ming-De Ke, Qing-Long Deng, and Kuan-Yao Chiu. Reduction of speckles and distortion in projection system by using a rotating diffuser. *Optical review*, 19(6):440–443, 2012.

[38] W. Goodman Joseph. *Speckle Phenomena in Optics: Theory and Applications*. Ben Roberts & Company, 2007.

[39] Dmitri Vladislavovich Kuksenkov, Shenping Li, Dragan Pikula, and Roussev Vatchev. Wavelength-switched optical systems, 2013.

[40] Jeffrey G. Manni and Joseph W. Goodman. Versatile method for achieving 1% speckle contrast in large-venue laser projection displays using a stationary multimode optical fiber. *Optics express*, 20(10):11288–11315, 2012.

[41] Matthias Busker. *Laser Projection: Coupling Optics, Light Management and Speckle Reduction*. VDM Verlag Dr. Muller Aktiengesellschaft & Co. Kg, 2008.

[42] Nan Ei Yu, Ju Won Choi, Heejong Kang, Do-Kyeong Ko, Shih-Hao Fu, Jiun-

Wei Liou, Andy H. Kung, Hee Joo Choi, Byoung Joo Kim, Myoungsik Cha, and Lung-Han Peng. Speckle noise reduction on a laser projection display via a broadband green light source. *Optics Express*, 22(3):3547, February 2014.

[43] Yoshihisa Ikeda, Yuji Takeda, Misaki Ueno, Yoshiaki Matsuba, Atsushi Heike, Yoji Kawasaki, and Junichi Kinoshita. Incoherentized high-brightness white light generated using blue laser diodes and phosphors-effect of multiple scattering. *Journal of Light & Visual Environment*, 37(2_3):95–100, 2013.

[44] Akio Furukawa, Norihiro Ohse, Yoshifumi Sato, Daisuke Imanishi, Kazuya Wakabayashi, Satoshi Ito, Koshi Tamamura, and Shoji Hirata. Effective speckle reduction in laser projection displays. pages 69110T–69110T–7, February 2008.

[45] Dinh Van Hoang, N. Thi Phuong, and Nguyen Van Phu. Random lasers: Characteristics, applications and some research results. *Computational Methods in Science and Technology*, pages 48–51, 2010.

[46] Matthias Liertzer and Stefan Rotter. Domesticating random lasers. *SPIE Newsroom*, September 2013.

[47] Brandon Redding, Michael A. Choma, and Hui Cao. Spatial coherence of random laser emission. *Optics Letters*, 36(17):3404–3406, September 2011.

[48] Brandon Redding, Michael A. Choma, and Hui Cao. Speckle-free laser imaging using random laser illumination. *Nature Photonics*, 6(7):496–496, July 2012.

[49] Brandon Redding, Hui Cao, and Michael A. Choma. Speckle-free laser imaging with random laser illumination. *Optics and Photonics News*, 23(12):30–30, December 2012.

[50] Guang Zheng, B. Wang, T. Fang, H. Cheng, Y. Qi, Y. W. Wang, B. X. Yan, Y. Bi, Y. Wang, S. W. Chu, and others. Laser digital cinema projector. *Display Technology, Journal of*, 4(3):314–318, 2008.

[51] J. Geske, C. Wang, and E. Burke. Multi-wavelength VCSEL array to reduce speckle, August 2013. WO Patent App. PCT/US2013/023,011.

[52] Nicholas George and Atul Jain. Speckle reduction using multiple tones of illumination. *Applied Optics*, 12(6):1202–1212, June 1973.

[53] Yunfang Zhang, Hui Dong, Rui Wang, Jingyuan Duan, Ancun Shi, Qing Fang, and Yuliang Liu. Demonstration of a home projector based on RGB semiconductor lasers. *Applied Optics*, 51(16):3584–3589, June 2012.

[54] A. Karpol, S. Reinhorn, E. Elysaf, S. Yalov, and B. Kenan. Method and apparatus for article inspection including speckle reduction, August 2005. US Patent 6,924,891.

[55] P.J. Kajenski, P.L. Fuhr, and D.R. Huston. Mode coupling and phase modulation in vibrating waveguides. *Journal of Lightwave Technology*, 10(9):1297–1301, September 1992.

[56] Jahja I. Trisnadi. Hadamard speckle contrast reduction. *Optics Letters*, 29(1):11–13, January 2004.

[57] Gaoming Li, Yishen Qiu, and Hui Li. Coherence theory of a laser beam passing through a moving diffuser. *Optics Express*, 21(11):13032, June 2013.

[58] Jui-Wen Pan and Chi-Hao Shih. Speckle reduction and maintaining contrast in a laser pico-projector using a vibrating symmetric diffuser. *Optics Express*, 22(6):6464, March 2014.

[59] Shigeo Kubota and Joseph W. Goodman. Very efficient speckle contrast reduction realized by moving diffuser device. *Applied optics*, 49(23):4385–4391, 2010.

[60] Jia Li. Design of optical engine for LCOS laser display with rotated diffuser plate. *Microwave and Optical Technology Letters*, 55(1):138–141, January 2013.

[61] T. Mizushima, H. Furuya, K. Mizuuchi, T. Yokoyama, A. Morikawa, K. Kasazumi, T. Itoh, A. Kurozuka, K. Yamamoto, S. Kadowaki, and others. L-9: Late-news paper: Laser projection display with low electric consumption and wide color gamut by using efficient green SHG laser and new illumination optics. In *SID Symposium Digest of Technical Papers*, volume 37, pages

1681–1684. Wiley Online Library, 2006.

[62] Seungdo An, Anatoliy Lapchuk, Victor Yurlov, Jonghyeong Song, HeungWoo Park, Jaewook Jang, Woocheol Shin, Sergey Karpoltsev, and Sang Kyeong Yun. Speckle suppression in laser display using several partially coherent beams. *Optics Express*, 17(1):92–103, January 2009.

[63] Lingli Wang, Theo Tschudi, Thorsteinn Halldorsson, and Palmi R. Petursson. Speckle reduction in laser projection systems by diffractive optical elements. *Applied Optics*, 37(10):1770–1775, April 1998.

[64] Guangmin Ouyang, Zhaomin Tong, M. Nadeem Akram, Kaiying Wang, Vladimir Kartashov, Xin Yan, and Xuyuan Chen. Speckle reduction using a motionless diffractive optical element. *Optics letters*, 35(17):2852–2854, 2010.

[65] Vladimir Kartashov and Muhammad Nadeem Akram. Speckle suppression in projection displays by using a motionless changing diffuser. *JOSA A*, 27(12):2593–2601, 2010.

[66] Fergal Shevlin. Speckle reduction with multiple laser pulses. *The 2nd Laser Display Conference, Yokohama, Japan, Apr. 23 - Apr. 24, 2013.*

[67] Stijn Roelandt, Youri Meuret, Gordon Craggs, Guy Verschaffelt, Peter Janssens, and Hugo Thienpont. Standardized speckle measurement method matched to human speckle perception in laser projection systems. *Optics express*, 20(8):8770–8783, 2012.

# Summary of Papers

## Journal papers

### 1. Design, Modeling and Characterization of a Microelectromechanical Diffuser Device for Laser Speckle Reduction

In this paper, a method for speckle suppression using MEMS diffuser device is presented. The device consists of random reflective patterns on top of a moving mass which is actuated for in plane vibration by electrostatic push-pull comb drive structure. The device is driven by the push-pull driving configuration in order to attain a pure sinusoidal vibration of the diffuser. The random patterns acts as a wavefront phase modulator. Due to the movement of the diffuser, the spatial phase of the incoming laser beam is varied thus time-varying speckle patterns are produced. These time variation of the speckle patterns are averaged due to the limit integration time of the human eyes; hence the speckle noise in the image is reduced. The speckle contrast measurement is performed with two different geometries which are freespace geometry and light pipe geometry. From the initial value, the speckle contrast is reduce by 43% for free space geometry and 26.8% for imaging geometry.

### 2. Speckle Reduction in Laser Projection using a Dynamic Deformable Mirror

This paper presents an approach for speckle reduction due to the angle diversity which is produced by dynamic deformable mirror. The dynamic deformable mirror

comprises of continuous micro-mirror array that can be individually deformed up to hundred of KHz. When the mirror is activated, many uncorrelated speckle patterns are produced due to the randomly distributed deformation of the micro-mirrors at high frequency. This leads to the reduction of speckle contrast in the projected image. Speckle suppression characterization are performed for red, blue broad-band lasers and green narrow band laser. Speckle contrast is brought down to 0.04 for broad band blue laser, 0.063 for broad band red laser and 0.09 for narrow band green laser.

**3. Speckle Reduction in Laser Projection Displays through Angle Diversity and Wavelength Diversity-Draft**

The speckle reduction for single laser through angle diversity using a dynamic deformable is presented in the previous paper. Further investigation of the effect of laser spectrum width by the use of multiple lasers on speckle reduction is discussed in this paper. Measurement of speckle contrast with and without angle diversity effects which is provided by deformable mirror is also performed for two and four lasers setups. The speckle contrast is also measured for both the same laser type or different laser types in the setup. Better speckle contrast suppression is provided by using multiple independent laser sources compared to single laser. Besides, it is also shown in this paper that the use of four lasers with a combination of two types of lasers offers better speckle contrast reduction than four lasers with the same type. Additional speckle contrast reduction is achieved by using a dynamic deformable mirror.

# Conference papers

### 1. Speckle Reduction Characterization of High Power Broad-area Edge Emitting Lasers

The investigation the speckle contrast reduction of high power broad-area edge-emitting red and blue lasers is performed. The speckle contrast is measured with different driving conditions. It can be observed from the measurement that the speckle contrast reduces with the increasing of pulse duration and pulse amplitude. The highest speckle contrast reduction that can be achieved with the red and the blue lasers are 27.9% and 10.4% respectively. The reduction of speckle contrast with the increasing of pulse amplitude and pulse duration is due to less coherence of laser beam as a result of more excited modes in the laser at higher current.

### 2. Demonstration of Speckle Reduction in a Laser Projector by Micro-electromechanical Diffuser Device

A demonstration of MEMS diffuser for speckle reduction in a commercial projector is presented in this paper. The demonstration is built on a *F2 SX+* wide projector from *Projectiondesign AS*. A blue laser Nichia NDB7675 with optical power $1.4W$ is used as a light source for the projector. The laser is driven at $1.2A$ at constant temperature $25^oC$. The laser beam is illuminated on the random surface of MEMS diffuser. The reflected beam from the diffuser is focused on the optic systems of the projector. After passing through the projector's system, a picture with laser light source is imaged on the screen by the projection lens for the characterization.

When the diffuser is at the stationary position, the speckle contrast value of the projected image is 0.4708. When the diffuser is activated to have displacement of $\pm 56.5\mu m$, the speckle contrast brought down to 0.3070. This corresponds to 34.8% of speckle reduction.

### 3. A Survey of Speckle Reduction Methods in Laser Based Picture Projectors

An overview of speckle suppression methods that have been reported in the literature is presented in this paper. Speckle noise in laser projection technology can be reduced by using time-sequential creation of many independent speckle patterns. Human eyes have integration time in the range of $30ms - 60ms$. By creating many independent speckle patterns that varies with time quickly, the speckle is reduced. The time varying speckle patterns can be generated by polymer dynamic diffraction grating, moving diffuser, vibrating mirror, rotating microlens array. Speckle can also be reduced by the creation of many independent speckle patterns which can be provided for example: by the use of array of independent lasers, the use of multimode optical fiber, broad spectrum laser, etc. The choice of speckle reduction methods depends on the choice of lasers sources and the architecture of the laser projector system.

**4. Design aspects for high lumne DLP Laser/Phosphor Projector**

The design and demonstration of a laser Digital Light Projector is presented in the paper. The laser demonstration system was built on a single chip DMD. The projector consists of 48 Nichia blue lasers and 74 red lasers from Mitsubishi. A Phosphor wheel was excited by the by the 8 blue laser banks from Nichia to get yellow color. Each laser bank has 8 individual laser diodes. The laser projector system provides about 10000 lumen. The speckle contrast characterization for the projection system is also presented in the paper.

Papers omitted from file due to publisher's regulations